Electronic Structure of Cycloheptatrienyl Sandwich Compounds of Actinides: An(η^7-C_7H_7)$_2$ (An = Th, Pa, U, Np, Pu, Am)

Jun Li and Bruce E. Bursten*

Contribution from the Department of Chemistry, The Ohio State University, Columbus, Ohio 43210

Received April 10, 1997. Revised Manuscript Received July 17, 1997[⊗]

Abstract: The cycloheptatrienyl actinide sandwich compounds An(η^7-C_7H_7)$_2^q$ (An = Th−Am; q = 2−, 1−, 0, 1+) have been studied by using local and gradient-corrected density functional methods, with the inclusion of scalar (mass−velocity and Darwin) relativistic effects. It has been found that the staggered conformer of U(η^7-C_7H_7)$_2^-$ is more stable than the eclipsed one by about 0.6 kcal/mol. The fδ orbitals not only participate in the bonding with the e_2'' pπ orbitals of the C_7H_7 rings, but are as important as the dδ orbitals in stabilizing the frontier pπ orbitals of the C_7H_7 rings. With increasing atomic number of the actinide, the 5f manifold and ligand based frontier MOs become considerably closer in energy. As a result, the actinide 5f percentage in the frontier e_2'' MOs increases markedly, while the contribution by the 6d orbitals gradually decreases. The ground electron configurations, ionization energies, electron affinities, and An−C_7H_7 bond energies are strongly affected by these effects. The bonding analysis indicates that U(η^7-C_7H_7)$_2^-$ and U(η^7-C_7H_7)$_2$ are best considered as complexes of U(III) and U(IV), respectively.

Introduction

The organometallic chemistry of the actinide (An) elements is dominated by complexes of η^n-C_nH_n ring ligands.[1−3] Developments during the past four decades have focused primarily on complexes of cyclopentadienyl (η^5-C_5H_5; Cp) and [8]-annulene (η^8-C_8H_8; COT) ligands, and of alkyl-substituted Cp and COT ligands. Unlike transition metal complexes of Cp, up to four Cp ligands can be bonded in pentahapto fashion to an actinide atom, leading to the well-known Cp_2AnX_2, Cp_3AnX, and Cp_4An complexes. COT has the remarkable capability of bonding in octahapto fashion to actinide elements, leading to the highly symmetric actinocene sandwich compounds An(COT)$_2$. Indeed, the 1968 synthesis of uranocene, U(COT)$_2$, is one of the milestones of modern organometallic chemistry.[4] More recently, organoactinide compounds that contain both Cp and COT ligands have been synthesized and structurally characterized.[5]

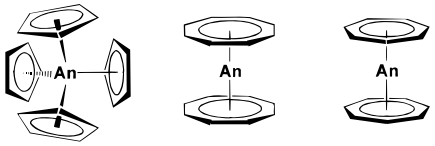

The bonding of Cp and COT ligands to actinide elements has been extensively investigated by using a variety of theoretical methods.[6−8] Not surprisingly, the bonding of these ligands to actinide elements is dominated by interactions of the ligand π orbitals with both the 5f and 6d orbitals of the actinide element. In fact, the bonding in uranocene was anticipated 5 years *before* the successful synthesis of the molecule, largely by consideration of the allowed interactions between the valence electrons of the uranium atom and the filled and empty π orbitals of the COT ligands.[9]

Recently, the class of organoactinide sandwich compounds has been expanded via the first report of a cycloheptatrienyl (η^7-C_7H_7; Ch) sandwich complex of an actinide element. This complex, the bis(cycloheptatrienyl)uranium anion (UCh_2^-), was synthesized and characterized crystallographically by Ephritikhine and co-workers.[10] The discovery of this anion paves the way for the exploration of the chemistry of cycloheptatrienyl sandwich compounds of actinides.

Prior studies of metal−Ch complexes have focused on mixed Cp−Ch complexes of the transition elements.[11] Most relevant to this contribution are the prior studies by Green, Green, Kaltsoyannis, and co-workers, who have used both theoretical

[⊗] Abstract published in *Advance ACS Abstracts,* September 1, 1997.

(1) (a) Marks, T. J. *Acc. Chem. Res.* **1976**, *9*, 223. (b) Marks, T. J. *Science* **1982**, *217*, 989. (c) Marks T. J.; Fischer, R. D., Eds. *Organometallics of f-Elements*; Reidel: Dordrecht, 1979.

(2) Some recent reviews: (a) Richter J.; Edelmann, F. T. *Coord. Chem. Rev.* **1996**, *147*, 373. (b) Cotton, S. A. *Annu. Rep. Prog. Chem., Sect. A: Inorg. Chem.* **1995**, *19*, 295−316; **1994**, *90*, 251−75; **1992**, *89*, 243−65. (c) Jones, C. J. *Annu. Rep. Prog. Chem., Sect. A: Inorg. Chem.* **1993**, *88*, 211−46; **1992**, *87*, 75−104. (d) Rogers R. D.; Rogers, L. M. *J. Organomet. Chem.* **1992**, *442*, 83−224; **1992**, *442*, 225−69; **1991**, *416*, 201−90.

(3) (a) Marks, T. J.; Streitwieser, A., Jr. In *The Chemistry of the Actinides Elements*; Katz, J. J., Seaborg, G. T., Morss, L. R., Eds.; Chapman and Hall: New York, 1986; Vol. 2, Chapter 22. (b) Marks, T. J. In *The Chemistry of the Actinides Elements*; Katz, J. J., Seaborg, G. T., Morss, L. R., Eds.; Chapman and Hall: New York, 1986; Vol. 2, Chapter 23.

(4) Müller-Westerhoff, U.; Streitwieser, A. D. *J. Am. Chem. Soc.* **1968**, *90*, 7364.

(5) Gilbert, T. M.; Ryan, R. R.; Sattelberger, A. P. *Organometallics* **1989**, *8*, 857.

(6) Bursten, B. E.; Strittmatter, R. J. *Angew. Chem.* **1991**, *103*, 1085; *Angew. Chem., Int. Ed. Engl.* **1991**, *30*, 1069.

(7) Some reviews of relativistic effects in actinide chemistry: (a) Pyykkö, P. *Inorg. Chim. Acta* **1987** *139*, 243. (b) Pepper, M.; Bursten, B. E. *Chem. Rev.* **1991**, *91*, 719. (c) Chang, A. H. H.; Zhao, K.; Ermler, W. C.; Pitzer, R. M. *J. Alloys Comp.* **1994**, *213/214*, 191. (d) Balasubramanian, K. In *Handbook on the Physics and Chemistry of Rare Earths*; Gschneider, K. A., Jr., Ering, L., Eds.; North-Holland: Amsterdam, 1994; Vol. 18, p 29. (e) Dolg, M. In *Handbook on the Physics and Chemistry of Rare Earths*; Gschneider, K. A., Jr.; Ering, L., Eds.; Elsevier Science Publishers B.V.: New York, 1995; Vol. 22. (f) Kaltsoyannis, N. *J. Chem. Soc., Dalton Trans.* **1997**, 1.

(8) Recent theoretical studies: (a) Rösch, N.; Streitwieser, A., Jr. *J. Am. Chem. Soc.* **1983**, *105*, 7237. (b) Rösch, N. *Inorg. Chim. Acta* **1984**, *94*, 297. (c) Boerrigter, P. M.; Baerends, E. J.; Snijders, J. G. *Chem. Phys.* **1988**, *122*, 357. (d) Chang A. H. H.; Pitzer, R. M. *J. Am. Chem. Soc.* **1989**, *111*, 2500. (e) Dolg, M.; Fulde, P.; Küchle, W.; Neumann, C.-S.; Stoll, H. *J. Chem. Phys.* **1991**, *94*, 3011. (f) King, R. B. *Inorg. Chem.* **1992**, *31*, 1978. (g) Cory, M. G.; Köstlmeier, S.; Kotzian, M.; Rösch, N.; Zerner, M. C. *J. Chem. Phys.* **1994**, *100*, 1353. (h) Dolg, M.; Fulde, P.; Stoll, H.; Preuss, H.; Chang, A. H. H.; Pitzer, R. M. *Chem. Phys.* **1995**, *195*, 71.

(9) Fischer, R. D. *Theor. Chim. Acta* (*Berlin*) **1963**, *1*, 418.

(10) Arliguie, T.; Lance, M.; Nierlich, M.; Vigner, J.; Ephritikhine, M. *J. Chem. Soc., Chem. Commun.* **1995**, *183*.

S0002-7863(97)01149-9 CCC: $14.00

calculations and photoelectron spectroscopy to provide an excellent description of the bonding in early-transition-metal ChMCp complexes.[12]

Inasmuch as UCh_2^- is the first bis(cycloheptatrienyl)metal sandwich compound,[13] its synthesis raises several interesting questions about this class of compounds: (1) Will other early actinides be able to form sandwich compounds with Ch ligands? (2) What are the most stable conformations of these molecules in the gas phase? (3) What are the electronic ground states of these complexes? (4) What are the best choices of the formal valence states of the actinide elements in these unique compounds? (5) What are the relative roles of the An 5f and 6d orbitals in stabilizing these complexes?

In this paper, we report theoretical investigations on the conformations, bonding, electronic states, stabilities, and energetics of cycloheptatrienyl sandwich compounds of the actinides Th through Am. We have focused on these actinides rather than the later ones because most of the early actinides have relatively long nuclear lifetimes, which can facilitate synthetic efforts in this area. Further, the chemical properties of the early actinides are distinctly different from those of the later actinides Cm−Lr.[14] Our calculations employ quasi-relativistic local-density and gradient-corrected density functional theory (DFT) methods,[15,16] which are less expensive computationally than correlated ab initio methods,[17] and can reach an accuracy comparable to the ab initio G1 procedure.[18] The complexes investigated include the neutral cycloheptatrienyl sandwich compounds $AnCh_2$ [Ch = η^7-C_7H_7; An = Th, Pa, U, Np, Pu, and Am], and the corresponding cations $AnCh_2^+$, monoanions $AnCh_2^-$, and dianions $AnCh_2^{2-}$. Because of the central role played by uranium in the development of organoactinide chemistry, particular attention is given to the isoelectronic series that include the UCh_2 and UCh_2^- complexes, namely the "20-electron (20e)" series $ThCh_2^{2-}$, $PaCh_2^-$, UCh_2, and $NpCh_2^+$, and the "21-electron (21e)" series $PaCh_2^{2-}$, UCh_2^-, $NpCh_2$, and $PuCh_2^+$.[19]

Computational Details

All the calculations were carried out with use of the Amsterdam Density Functional (ADF) code, Versions 1.1 and 2.0 (Theoretical Chemistry, Vrije Universiteit, Amsterdam, The Netherlands), developed by Baerends et al.,[20] which incorporates the relativistic extensions first proposed by Snijders et al.[21] The code was vectorized by Ravenek,[22] and the numerical integration scheme applied for the calculations was developed by te Velde et al.[23] The density functional calculations were performed by using the non-relativistic local density approach (LDA^{NR}),[24] the relativistic local density approach (LDA^{R}),[25] and the gradient-corrected method that utilized Becke's exchange functional[26] and Perdew's correlation functional[27] (BP^{NR} and BP^{R}). Most calculations were carried out by using the spin-restricted Kohn−Sham (RKS) method to facilitate bonding discussion and to reduce the computational cost. However, for some of the one-electron properties, the spin-unrestricted Kohn−Sham (UKS) density functional calculations were used as well. All the results presented were taken from the RKS calculations, except as otherwise specified.

The basis set for the actinide atoms consists of uncontracted triple-ζ STO bases for the 6d and 5f AOs, uncontracted double-ζ STO bases for the 6s, 6p, and 7s AOs, and a single-ζ STO basis for the 7p AOs. For the ligand-based orbitals, we use uncontracted double-ζ STO bases for the 2s and 2p orbitals of carbon and for the 1s orbital of hydrogen.[28] The $1s^2$ core of carbon and the $[Xe]4f^{14}5d^{10}$ cores of the actinides were treated by using the frozen-core approximation proposed by Baerends and co-workers.[20a] For fitting the molecular density and accurately representing the Coulomb and exchange potentials in each SCF cycle, a set of auxiliary s, p, d, f, and g type STO functions centered on all nuclei were used.[29] The scalar relativistic effects, i.e. the mass−velocity effect and the Darwin effect, were taken into account by use of the quasi-relativistic method[30] incorporated in the ADF calculations. The relativistic atomic core densities and the core potentials for the actinide and the carbon atoms were computed by using the ADF auxiliary program DIRAC.

The geometries of these compounds were optimized by using the analytical energy gradient techniques implemented in ADF 2.0. All An−C, C−C, and C−H distances and the angle between the C−H bonds and the C_7 plane were fully optimized under the constraint of D_{7h} symmetry. Tight criteria for the numerical integration accuracy (INTEGRATION = 4.0) and the gradient convergence (10^{-4}) were adopted for the geometry optimizations.

Results and Discussion

Free Ligand Calculations. One of the goals in this study is to assess the donor and acceptor capabilities of the Ch ligand

(11) For cycloheptatrienyl compounds of transition metals, see: (a) Deganello, G. *Transition Metal Complexes of Cyclic Polyolefins*; Academic Press: London, 1979; Chapter 1. (b) Green, M. L. H.; Ng, D. K. P. *Chem. Rev.* **1995**, *95*, 439.

(12) (a) Green, J. C.; Green, M. L. H.; Kaltsoyannis, N.; Mountford, P.; Scott P.; Simpson, S. J. *Organometallics* **1992**, *11*, 3353. (b) Green, J. C.; Kaltsoyannis, N.; Sze, K. H.; MacDonald, M. *J. Am. Chem. Soc.* **1994**, *116*, 1994. (c) Kaltsoyannis, N. *J. Chem. Soc., Dalton Trans*. **1995**, 3727.

(13) Although $V(C_7H_7)_2^{2+}$ is found in mass spectra, it is not clear whether it is a sandwich compound. See: Müller J.; Mertschenk, B. *Chem. Ber*. **1972**, *105*, 3346. For actinide and lanthanide elements, cycloheptatrienyl trianion compounds have been prepared as well: Miller, J. T.; DeKock, C. W. *J. Organomet. Chem*. **1981**, *216*, 39.

(14) (a) Cotton, F. A.; Wilkinson, G. *Advanced Inorganic Chemistry*, 5th ed.; John Wiley & Sons, Inc.: New York, 1988; Chapter 21. (b) Katz, J. J.; Morss, L. R.; Seaborg, G. T. In *The Chemistry of the Actinides Elements*, 2nd ed.; Katz, J. J., Seaborg, G. T., Morss, L. R., Eds.; Chapman and Hall: New York, 1996; Vol. 2, Chapter 14.

(15) (a) Hohenberg, P.; Kohn, W. *Phys. Rev*. **1964**, *B136*, 864. (b) Kohn, W.; Sham, L. J. *Phys. Rev.* **1965**, *A140*, 1133.

(16) (a) Parr, R. G.; Yang, W. *Density Functional Theory of Atoms and Molecules*; Oxford University: New York, 1989. (b) Dreizler, R. M.; Gross, E. K. U. *Density Functional Theory*; Springer: Berlin, 1990. (c) Kryachko, E. S.; Ludeña, E. V. *Energy Density Functional Theory of Many-Electron Systems*; Kluwer: Dordrecht, 1990. (d) Labanowski, J. K., Andzelm, J. W., Eds.; *Density Functional Methods in Chemistry*; Springer: New York, 1991. (e) Gross, E. K. U.; Dreizler, R. M. *Density Functional Theory*; Plenum: New York, 1995. (f) Seminario, J. M., Politzer, P., Eds. *Modern Density Functional Theory: A Tool for Chemistry*; Elsevier: Amsterdam, 1995. (g) Ellis, D. E., Ed. *Density Functional Theory of Molecules, Clusters, and Solids*, Kluwer Academic Publishers: Dordrecht, 1995.

(17) See, for example: Johnson, B. G.; Gill, P. M. W.; Pople, J. A. *J. Chem. Phys*. **1992**, *97*, 7846.

(18) For lighter molecules, see: Becke, A. D. *J. Chem Phys*. **1992**, *96*, 2155. Good accuracy can also be reached for heavier systems such as transition metals and lanthanides. See, for example: (a) Eriksson, L. A.; Pettersson, L. G. M.; Siegbahn, P. E. M.; Wahlgren, U. *J. Chem. Phys*. **1995**, *102*, 872. (b) Wang, S. G.; Schwarz, W. H. E. *J. Phys. Chem*. **1995**, *99*, 11687.

(19) The 20e and 21e electron counts are derived in the "usual" way that organometallic complexes of cyclohydrocarbyl ligands are derived. The electrons included in the count are the π electrons of the Ch ligands and the valence electrons of the An atom.

(20) (a) Baerends, E. J.; Ellis, D. E.; Ros, P. *Chem. Phys*. **1973**, *2*, 42. (b) Baerends, E. J.; Ros, P. *Chem. Phys*. **1973**, *2*, 51. (c) Baerends, E. J.; Ros, P. *Int. J. Quantum Chem.* **1978**, *S12*, 169.

(21) (a) Snijders, J. G.; Baerends, E. J. *J. Mol. Phys.* **1978**, *36*, 1789. (b) Snijders, J. G.; Baerends, E. J.; Ros, P. *Mol. Phys*. **1979**, *38*, 1909.

(22) Ravenek, W. In *Algorithms and Applications on Vector and Parallel Computes*; te Riele, H. J. J., DeDekker, Th. J., van de Vorst, H. A., Eds.; Elsevier: Amsterdam, 1987.

(23) (a) Boerrigter, P. M.; te Velde, G.; Baerends, E. J. *Int J. Quantum Chem.* **1988**, *33*, 87. (b) te Velde, G.; Baerends, E. J. *J. Comput. Phys*. **1992**, *99*, 94.

(24) For the LDA exchange part, see, for example: Ziegler, T. *Chem. Rev*. **1991**, *91*, 651. For the LDA correlation part, see: Vosko, S. H.; Wilk, L.; Nusair, M. *Can. J. Phys*. **1980**, *58*, 1200.

(25) (a) Ziegler, T.; Snijders, J. G.; Baerends, E. *J. Chem. Phys*. **1981**, *74*, 1271. (b) Boerrigter, P. M. Ph.D. Thesis, Vrije Universiteit, Amsterdam, 1987.

(26) Becke, A. D. *Phys. Rev.* **1988**, *A38*, 3098.

(27) Perdew, J. P. *Phys. Rev*. **1986**, *B33*, 8822; **1986**, *B34*, 7406 (erratum).

(28) (a) Snijders, J. G.; Baerends, E. J.; Vernooijs, P. *At. Nucl. Data Tables* **1982**, *26*, 483. (b) Vernooijs, P.; Snijders, J. G.; Baerends, E. J. *Slater Type Basis Functions for the Whole Periodic System*; Internal Report, Free University of Amsterdam, The Netherlands, 1984.

(29) Krijn, J.; Baerends, E. J. *Fit Functions in the HFS Method*; Internal Report, Free University of Amsterdam, The Netherlands, 1984.

(30) Ziegler, T.; Baerends, E. J.; Snijders, J. G.; Ravenek, W. *J. Phys. Chem*. **1989**, *93*, 3050.

Table 1. Character Table for the D_{7h} Point Group[a]

D_{7h}	E	$2C_7$	$2C_7^2$	$2C_7^3$	$7C_2$	σ_h	$2S_7$	$2S_7^3$	$2S_7^5$	$7\sigma_v$	An orbitals	$(Ch)_2$ orbitals[b]
A_1'	1	1	1	1	1	1	1	1	1	1	s, d_0	π_0'
A_2'	1	1	1	1	−1	1	1	1	1	−1		
E_1'	2	2α	2β	2γ	0	2	2α	2γ	2β	0	$p_{\pm1}$, $f_{\pm1}$	π_1'
E_2'	2	2β	2γ	2α	0	2	2β	2α	2γ	0	$d_{\pm2}$	π_2'
E_3'	2	2γ	2α	2β	0	2	2γ	2β	2α	0	$f_{\pm3}$	π_3'
A_1''	1	1	1	1	1	−1	−1	−1	−1	−1		
A_2''	1	1	1	1	−1	−1	−1	−1	−1	1	p_0, f_0	π_0''
E_1''	2	2α	2β	2γ	0	−2	−2α	−2γ	−2β	0	$d_{\pm1}$	π_1''
E_2''	2	2β	2γ	2α	0	−2	−2β	−2α	−2γ	0	$f_{\pm2}$	π_2''
E_3''	2	2γ	2α	2β	0	−2	−2γ	−2β	−2α	0		π_3''

[a] $\alpha = \cos(2\pi/7)$, $\beta = \cos(4\pi/7)$, $\gamma = \cos(6\pi/7)$. [b] The notations π_i' and π_i'' refer to group orbitals of the π_i orbitals of the two Ch rings that are symmetric and antisymmetric with respect to the σ_h mirror plane, respectively.

relative to more familiar ligands for actinides, such as Cp and COT. Planar cyclic η^n-C_nH_n ligands, such as Cp, benzene, and COT, interact with metal atoms primarily via the ligand's filled and empty π MOs. Not surprisingly, we will see that this is also the case for the Ch ligand. It will also be of interest to address the question of what is the best choice of formal charge for the Ch ligand in the complexes. In the case of Cp and COT, it is clear that these ligands are best considered as the Hückel-aromatic 6e$^-$ $C_5H_5^-$ and 10e$^-$ $C_8H_8^{2-}$ anions, respectively. Thus, both Cp_4U and $U(COT)_2$ are best considered as f^2 U(IV) complexes.

We will consider the free ligand under its most symmetric heptagonal planar geometry, for which it will have D_{7h} point symmetry. Because D_{7h} symmetry is rather uncommon, this point group is not generally included in compilations of character tables. We present the character table for the D_{7h} single group in Table 1, along with the representations spanned by relevant orbitals of the $AnCh_2$ systems. Under D_{7h} symmetry, the pπ AOs of C_7H_7 lead to the following π MOs, in order of increasing energy: a_2'' (π_0) < e_1''(π_1) < e_2''(π_2) < e_3''(π_3). Contour diagrams of these π MOs are presented in Figure 1. As is typical for symmetric, planar π systems, the pπ AO coefficients for each of these MOs can be determined entirely from the irreducible representations of the D_{7h} point group.[31]

The Ch ligand lends itself to two limiting $4n + 2$ π-electron forms, namely as a 6e$^-$ $C_7H_7^+$ ion or as a 10e$^-$ $C_7H_7^{3-}$ ion. Figure 2 compares the relative energies of the π MOs of the 6e$^-$ systems $C_4H_4^{2-}$, $C_5H_5^-$, C_6H_6, $C_7H_7^+$, and $C_8H_8^{2+}$, and of the 10e$^-$ systems $C_6H_6^{4-}$, $C_7H_7^{3-}$, and $C_8H_8^{2-}$ as obtained via BP^R ADF calculations with double-ζ basis sets. Because the charges on the systems are different, the MO energies cannot be compared directly; rather, the orbital energies are referenced to the lowest-lying totally-symmetric orbital in each molecule or ion.

The results in Figure 2 are in accord with the expectations from usual π-only treatments of cyclic C_nH_n systems, and with prior studies of the bonding capabilities of the Ch ligand.[12] In the 6e$^-$ systems, the doubly-degenerate HOMO acts as a donor orbital to the An orbitals and the LUMO (singly-degenerate for $C_4H_4^{2-}$, doubly-degenerate for the others) acts as an acceptor orbital. For $C_7H_7^+$, the e_1'' HOMO and e_2'' LUMO are, as expected, significantly lower in energy than the corresponding MOs in $C_5H_5^-$ and C_6H_6; in particular, the e_2'' orbital of $C_7H_7^+$ is ca. 3.7 eV lower in energy than the e_2'' MO in $C_5H_5^-$. Thus, $C_7H_7^+$ will act as a weaker donor ligand and a significantly stronger acceptor ligand than does $C_5H_5^-$ or C_6H_6. In the 10e$^-$ $C_7H_7^{3-}$ anion, the filled e_2'' MO is the HOMO of the ion and acts as a donor orbital. This orbital is roughly 0.7 eV higher than the corresponding e_{2u} MO of $C_8H_8^{2-}$, and therefore the $C_7H_7^{3-}$ ion is expected to be a stronger donor ligand than

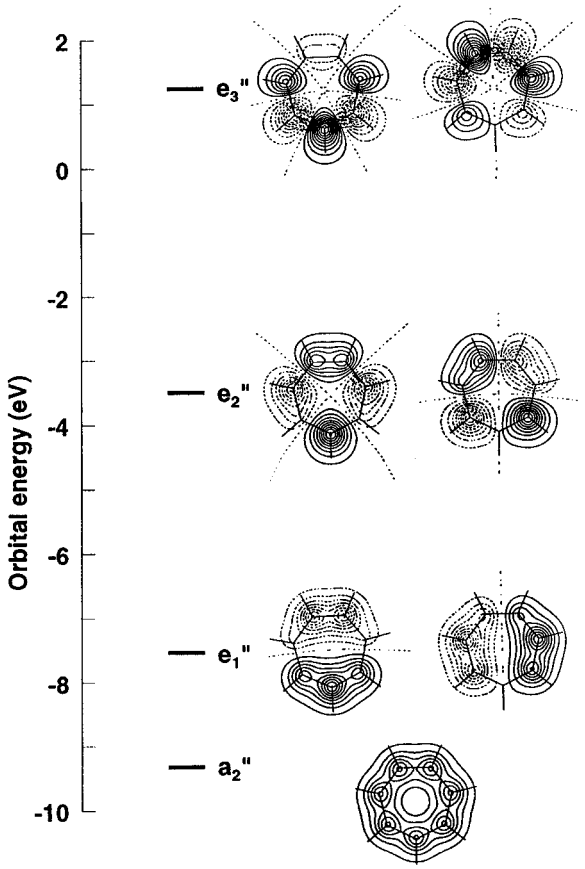

Figure 1. Contour diagrams of the π MOs of planar C_7H_7 taken 0.5 Å above the molecular plane. Contour values are $\pm n \cdot 0.05$ Å$^{-3/2}$, with negative contours indicated with dashed lines.

$C_8H_8^{2-}$. These observations suggest that the Ch ligand is less likely to act as a $4n + 2$ π electron ligand than is either Cp or COT, and that the "best" charge on the ligand in $AnCh_2$ complexes may be intermediate between the Hückel extremes of 1+ and 3−.

Qualitative Aspects of the Bonding in $AnCh_2$ Complexes. Before discussing the quantitative results of the calculations on $AnCh_2$ complexes, it is useful to present a qualitative discussion of the bonding in these complexes, driven largely by their high symmetry. For this discussion, we will assume that both the free Ch ligand and the $AnCh_2$ complexes have D_{7h} symmetry, which corresponds to an eclipsed conformation for the complexes. This discussion can readily be extended to staggered (D_{7d}) or semistaggered (D_7) conformations of $AnCh_2$, but we will not present those extensions here.

The representations spanned by relevant orbitals of the $AnCh_2$ systems are presented in Table 1. Because of the cylindrical symmetry of the complexes, it is convenient to label the AOs of the An atoms by using the magnetic angular quantum number

(31) For the symmetry aspects of the π MOs for cyclopolyenes and cyclopolyenyls, see, for example: Cotton, F. A. *Chemical Applications of Group Theory*, 3rd ed.; Wiley: New York, 1990.

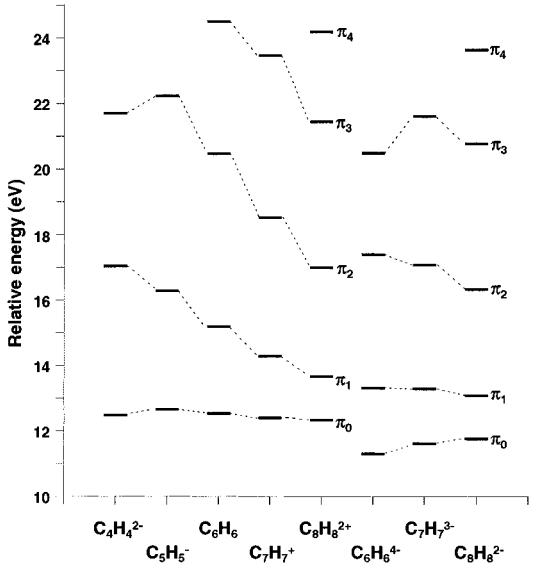

Figure 2. Relative energies of the π MOs of the 6e$^-$ systems $C_4H_4^{2-}$, $C_5H_5^-$, C_6H_6, $C_7H_7^+$, and $C_8H_8^{2+}$, and of the 10e$^-$ systems $C_6H_6^{4-}$, $C_7H_7^{3-}$, and $C_8H_8^{2-}$. All MO energies are referenced to the lowest totally-symmetric MO in each molecule or ion.

(m_l) rather than the usual Cartesian labels. Under this system, the real orbitals corresponding to the complex orbitals of $m_l = 0, \pm1, \pm2$, and ±3 are of σ, π, δ, and ϕ symmetry with respect to the An−Ch bonding. Therefore, the orbitals f_{z^3}, $\{f_{xz^2}, f_{yz^2}\}$, $\{f_{z(x^2-y^2)}, f_{xyz}\}$, and $\{f_{x(x^2-3y^2)}, f_{y(3x^2-y^2)}\}$ will be represented by f_0, $f_{\pm1}$, $f_{\pm2}$, and $f_{\pm3}$, respectively. This notation has several advantages: (1) The D_{7h} and D_{7d} ligand fields do not mix orbitals of different $|m_l|$ values. (2) The subscripts of p, d, and f orbitals with $|m_l| > 0$ match those of the doubly-degenerate irreducible representations of the $(C_7H_7)_2$ pπ orbitals. (3) In a double group formalism, the splittings due to spin−orbit coupling are easily obtained when the complex spherical harmonics Y_l^m and Y_l^{-m} ($|m| = \lambda$) are used as basis functions. We will present double-group results in a later publication.

Combinations of the π MOs on two eclipsed Ch rings lead to group orbitals that are symmetric and antisymmetric with respect to the mirror plane that is perpendicular to the C_7 axis. In Table 1, these symmetric and antisymmetric combinations are denoted π_i' and π_i'', respectively.

The extent of interaction between the metal-based d and f orbitals and the appropriate ring orbitals will be governed by the overlap of these orbitals and by their energetic closeness. The d_0 (dσ) and f_0 (fσ) orbitals are directed along the C_7 axis, but are required to interact with the lowest energy π orbitals, those derived from π_0. These orbitals are expected to be significantly lower in energy than the An orbitals, leading to only a weak interaction. The An $d_{\pm1}$ (dπ), $f_{\pm1}$ (fπ), and $f_{\pm2}$ (fδ) AOs have lobes that are directed at the Ch π_1 and π_2 MOs. The $f_{\pm3}$ (fϕ) orbitals will suffer from poor overlap with the energetically-high Ch π_3 orbitals, and should therefore also interact only weakly. The $d_{\pm2}$ (dδ), although lying in the *xy*-plane, are expected to be diffuse enough to interact substantially with the energetically-favorable Ch π_2 orbitals. Thus, we expect the greatest interaction to involve the d and f orbitals with $m_l = \pm1$ or ±2, as shown in Figure 3.

Orbital Energetics in UCh_2. To illustrate the general features of the bonding between an actinide atom and two C_7H_7 ligands, we present results for a prototypical 20-electron complex, UCh_2. We have chosen neutral UCh_2 rather than the known UCh_2^- anion because the former can exist in a closed-shell ($^1A_1'$) state; further, this choice avoids the complexity caused by electron occupations among nearly degenerate 5f orbitals (*vide infra*). The correlation diagram for the interaction

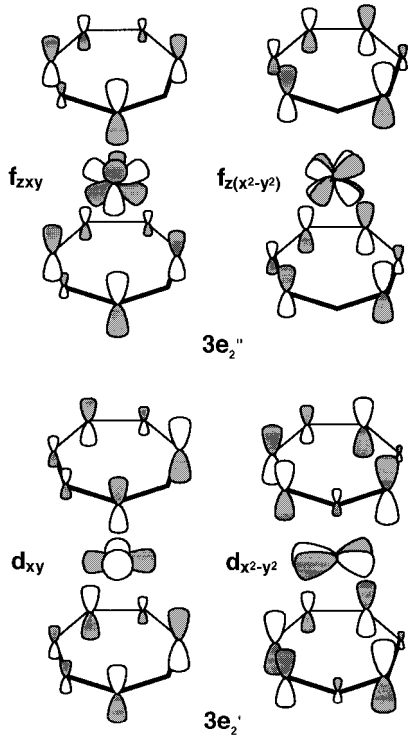

Figure 3. Sketches of the dominant bonding interactions between C_7H_7 and the appropriate An d and f orbitals in $AnCh_2$.

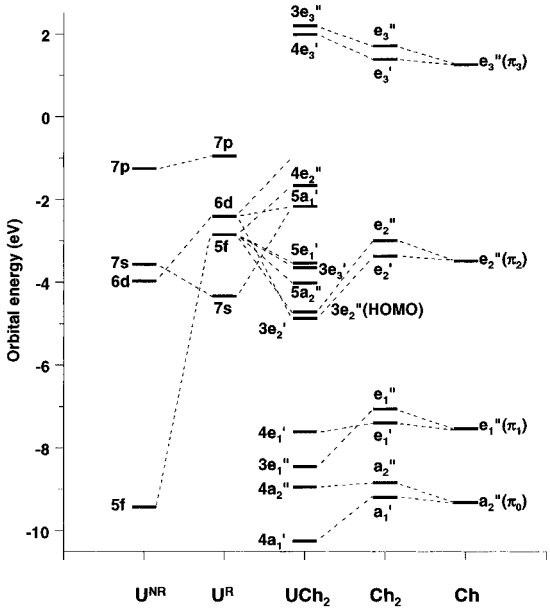

Figure 4. Correlation diagram for the interaction of the orbitals of U and two C_7H_7 ligands under D_{7h} symmetry. U^{NR} and U^R indicate atomic orbital energies at the nonrelativistic and relativistic levels, respectively. The results for UCh_2 include realtivistic corrections.

of the orbitals of U and two C_7H_7 ligands under D_{7h} symmetry is depicted in Figure 4. The orbital energies used to construct this figure are taken from BP^{NR} and BP^R calculations of the U atom, and BP^R calculations for the Ch, Ch_2, and UCh_2 species fixed at the experimental geometry of UCh_2^-.

Figure 4 makes evident some of the challenges in calculations on $AnCh_2$ complexes. First, we note that the one-electron relativistic effects serve to destabilize both the An 5f and 6d AOs, the former more than the latter. For U and other early actinides, these effects cause the 5f and 6d orbitals to be in close energetic proximity, allowing both to participate significantly in bonding. Second, unlike the corresponding MOs in Cp, C_6H_6, and COT, the e_2'' (π_2) MO of the Ch ring, due to its

weakly antibonding nature, is at nearly the same energy as the valence orbitals on U. This energetic closeness is expected to enhance the interaction between the Ch π_2 MOs and the actinide AOs.

As anticipated from the above discussion, the most important metal−ligand interactions in UCh_2 are between the 6dδ and 6fδ and the appropriate Ch π_2 group orbitals. The 6dδ AOs interact with the π_2' orbital to produce the $3e_2'$ MO of UCh_2, and the 6fδ AOs interact with the π_2'' orbital, yielding the $3e_2''$ MO. These MOs involve substantial mixing between the U and Ch orbitals, much as they do in the calculations by Kaltsoyannis on transition-metal ChMCp systems.[12c] In the $^1A_1'$ state of UCh_2, the $3e_2'$ and $3e_2''$ MOs are completely filled, with the $3e_2''$ MO serving as the HOMO of the complex.

Immediately above the $3e_2'$ and $3e_2''$ MOs of UCh_2 is a closely-spaced set of empty, primarily 5f-based MOs. We can therefore anticipate that UCh_2 and other $AnCh_2$ systems will have a high density of electronic states close to the ground state. Therefore, to determine the ground electron distribution in these actinide compounds, it is necessary to calculate the energies of a large number of different electron configurations. We will now address the ground configurations of some of these complexes before discussing their calculated geometries.

Ground Configurations. A complete discussion of the ground states of $AnCh_2$ complexes requires a double-group treatment involving spin−orbit coupling. The inclusion of spin−orbit effects will be particularly important for assigning optical transitions in these systems. We are presently exploring this double-group description of the ground states, and we will not present any of those results here. Rather, we shall examine some of the trends in low-lying electron configurations as a function of actinide metal, discussed in a single-group framework with the inclusion of scalar relativistic corrections.[32]

Our discussion of configurations will focus on the 20e systems, such as UCh_2, and the 21e systems, of which the known system UCh_2^- is an example. Most of the configuration energies reported here are at the BP^R optimized geometry of the complex in question. The optimized geometries will be discussed in the next section.

The isoelectronic 20e systems that we have examined are $ThCh_2^{2-}$, $PaCh_2^-$, UCh_2, and $NpCh_2^+$. As noted in the MO diagram for UCh_2 in Figure 4, these systems have the correct number of electrons to fill completely the $3e_2'$ and $3e_2''$ MOs. These MOs represent strong bonding interactions between the π_2 orbitals of the Ch rings and the An 6d and 5f AOs, respectively, and for these systems, the $3e_2'$ MO is somewhat lower in energy than the $3e_2''$ MO. We will represent the closed-shell configuration in which the $3e_2'$ and $3e_2''$ MOs are completely filled as the $(e_2')^4(e_2'')^4$ configuration.

On the basis of Figure 4, the lowest open-shell configurations are expected to involve the transfer of an electron from the $3e_2''$ MO to the low-lying An 5f- or 6d-localized MOs that are immediately above the $3e_2''$ MO. For Th, the 6d AOs are lower in energy than the 5f AOs; however, as we progress from Th to the later actinide elements, the energies of the 6d orbitals increase slightly, while those of the 5f orbitals markedly decrease.[33,34] We have therefore considered some of the states derived from the $(e_2')^4(e_2'')^3f^1$, $(e_2')^3(e_2'')^4f^1$, $(e_2')^4(e_2'')^3d^1$, and $(e_2')^3(e_2'')^4d^1$ open-shell configurations of the 20e systems. In accord with Figure 4, the lowest energy in the open-shell configurations is obtained when the 5f- or 6d-localized electron is placed in the $5a_2''$ (f_0) or $5a_1'$ (d_0) MO relative to other 5f- and 6d-localized MOs.

Table 2. Restricted Average-of-Configuration BP^R Relative Energies (eV) at the Optimized Geometries for the Low-Lying Outer Electron Configurations of 20e and 21e Isoelectronic Series of $AnCh_2^q$ Complexes

		20e systems			
configuration	state	$ThCh_2^{2-}$	$PaCh_2^-$	UCh_2	$NpCh_2^+$
$(e_2')^4(e_2'')^4$	A_1'	0	0	0	0
$(e_2')^4(e_2'')^3(d_0)^1$	E_2''	1.46	2.14	2.75	3.55
$(e_2')^3(e_2'')^4(d_0)^1$	E_2'	2.07	2.59	2.73	2.70
$(e_2')^4(e_2'')^3(f_0)^1$	E_2'	2.63	1.89	0.86	0.15
$(e_2')^3(e_2'')^4(f_0)^1$	E_2''	3.35	2.59	1.22	−0.13

		21e systems			
configuration	state	$PaCh_2^{2-}$	UCh_2^-	$NpCh_2$	$PuCh_2^+$
$(e_2')^4(e_2'')^4(f_0)^1$	A_2''	0	0	0	0
$(e_2')^4(e_2'')^3(f_0)^1(f_{\pm3})^1$	$E_1' + E_2'$	2.77	1.67	0.85	0.24
$(e_2')^3(e_2'')^4(f_0)^1(f_{\pm3})^1$	$E_1'' + E_2''$	3.45	2.20	1.00	−0.31

The relative BP^R energies of the states of the 20e $AnCh_2$ systems are given in Table 2. The closed-shell $(e_2')^4(e_2'')^4$ configuration is the lowest one for $ThCh_2^{2-}$, $PaCh_2^-$, and UCh_2. As expected, the $(e_2')^4(e_2'')^3(d_0)^1$ and $(e_2')^3(e_2'')^4(d_0)^1$ configurations generally increase in energy relative to the ground configuration as we proceed from Th through Np, which reflects the increasing energy of the An 6d AOs. At the same time, the $...(f_0)^1$ configurations become lower in energy as the 5f AOs drop in energy. For $NpCh_2^+$, the energy of the Np 5f has become low enough that we predict an E_2'' ground state derived from the $(e_2')^3(e_2'')^4(f_0)^1$ open-shell configuration.[35] It is interesting that, for $NpCh_2^+$, the $(e_2')^3(e_2'')^4(f_0)^1$ configuration leads to a lower energy than does the $(e_2')^4(e_2'')^3(f_0)^1$ configuration; for this system, the 5f orbitals are sufficiently lower than the 6d orbitals to make it more favorable to depopulate the e_2' rather than the e_2'' MO.

For the 21e systems, we will start with the known anion UCh_2^-. On the basis of the MO diagram in Figure 4, we expect the lowest-energy configurations to be those in which the $3e_2'$ and $3e_2''$ MOs are completely filled, with the remaining electron residing in one of the U 5f- or 6d-localized orbitals. We examined this anion at its experimental geometry, at state-optimized geometries, and as eclipsed (D_{7h}) and staggered (D_{7d}) rotamers. We will discuss the relative energies of the rotamers in the next section; for now, we will discuss the D_{7h} results.

(32) Our preliminary calculations that include spin-orbit effects provide support for the neglect of these effects for the properties discussed in this paper. For example, the strong metal−ligand bonding MOs of UCh_2^-, the $3e_2'$ and $3e_2''$ MOs, are split by only about 0.1 eV by spin−orbit coupling. The 5f-localized MOs are affected more, but not to an extent that the ordering of states is drastically changed. For example, the double-group ground state determined for UCh_2^- has the $(e_{13/2})^1$ configuration, which corresponds directly to the single-group ground state, $(a_2'')^1$, inasmuch as the $e_{13/2}$ orbital is derived principally from the U $5f_0$ single-group orbital. We expect that the inclusion of these effects would not cause any significant change in the geometries calculated in this paper.

(33) Experimental results: (a) Brewer, L. *J. Opt. Soc. Am.* **1971**, *61*, 1666. (b) Brooks, M. S. S.; Johansson, B.; Skriver, H. L. In *Handbook on the Physics and Chemistry of the Actinides*; Freeman, A. J., Lander, G. H., Eds.; North-Holland: Amsterdam, 1984; Vol. 1, Chapter 3. (c) Fred, M. S. In *The Chemistry of the Actinides Elements*, 2nd ed.; Katz, J. J., Seaborg, G. T., Morss, L. R., Eds.; Chapman and Hall: New York, 1986; Vol. 2, Chapter 15. (d) Carnall, W. T.; Crosswhite, H. M. In *The Chemistry of the Actinides Elements*, 2nd ed.; Katz, J. J., Seaborg, G. T., Morss, L. R., Eds.; Chapman and Hall: New York, 1986; Vol. 2, Chapter 16, 1986.

(34) For theoretical results see, for example: (a) Pyykkö, P.; Laakkonen, L. J.; Tatsumi, K. *Inorg. Chem.* **1989**, *28*, 1801. (b) Bagnall, K. W. *The Actinide Elements*; Elsevier Publishing Company: Amsterdam, 1972; Chapter 1.

(35) Because the calculations on the two-open-shell configurations have been carried out in the restricted Kohn−Sham (RKS) formalism, the spin quantum numbers for the resultant states are ambiguous. The state energies are multiplet averages of the pure singlet and triplet states. In principle, the pure triplet state energy could be obtained from unrestricted Kohn−Sham (UKS) calculations. However, upon the inclusion of spin−orbit coupling, the notion of singlet and triplet states becomes less relevant so we report only the RKS results for these configurations.

Table 3. Relative Energies (eV) for Nine Low-Lying Outer Electron Configurations of UCh_2^- under Eclipsed (D_{7h}) and Staggered (D_{7d}) Geometries[a]

	D_{7h}			D_{7d}		
configuration[b]	LDA^{NR}	LDA^{R}	BP^{R}	LDA^{NR}	LDA^{R}	BP^{R}
$(e_2')^4(e_2'')^4(f_0)^1$	0	0	0	−0.030	−0.033	−0.030
$(e_2')^4(e_2'')^4(f_{\pm1})^1$	0.56	0.44	0.51	0.53	0.42	0.49
$(e_2')^4(e_2'')^4(f_{\pm3})^1$	0.49	0.47	0.54	0.47	0.45	0.52
$(e_2')^4(e_2'')^4(d_0)^1$	3.21	1.34	1.46	3.19	1.31	1.44
$(e_2')^4(e_2'')^3(f_0)^1(f_{\pm3})^1$	0.92	1.83	1.86	0.89	1.81	1.84
$(e_2')^4(e_2'')^3(f_0)^2$	1.16	1.97	1.88	1.12	1.93	1.84
$(e_2')^4(e_2'')^4(f_{\pm2})^1$	2.34	1.88	1.90	2.31	1.86	1.87
$(e_2')^3(e_2'')^4(f_0)^1(f_{\pm3})^1$	1.02	2.47	2.46	0.99	2.43	2.43
$(e_2')^3(e_2'')^4(f_0)^2$	1.29	2.65	2.53	1.25	2.60	2.49

[a] All calculations were carried out by using the experimental U−C (2.53 Å) and C−C (1.37 Å) bond lengths. [b] Under D_{7d} symmetry, the e_2' and e_2'' orbitals transform as e_{2g} and e_{2u}, respectively.

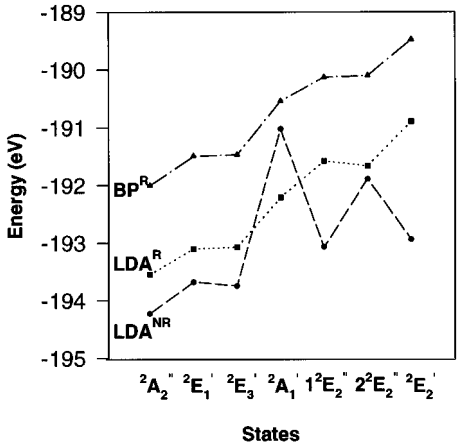

Figure 5. The eclipsed-rotamer energies for different electronic states of UCh_2^- at various levels of calculation. The BP^R energies have all been made more negative by 15 eV for convenience of display.

The LDA^{NR}, LDA^R, and BP^R energies of the various configurations, using the experimental bond lengths, are presented in Table 3 for both eclipsed and staggered rotamers. The eclipsed-rotamer energies at the various levels of calculation are plotted in Figure 5 for those configurations that lead to unambiguous doublet states; we have excluded the multiple open-shell configurations $(e_2')^3(f_0)^1(f_{\pm3})^1$ and $(e_2'')^3(f_0)^1(f_{\pm3})^1$.

Several features of the plots in Figure 5 are notable. First, the inclusion of relativistic effects drastically changes the ordering of the states, largely because of differential effects on the 5f and 6d AOs of the U atom. The two relativistic methods give very comparable relative energies. We see that all three levels of calculation predict a $^2A_2''$ ground state that corresponds to the $(e_2')^4(e_2'')^4(f_0)^1$ electron configuration, which is predicted on the basis of the MO diagram in Figure 4. The two lowest-lying excited states, which are nearly degenerate, are the $^2E_3'$ and $^2E_1'$ states that also correspond to $(e_2')^4(e_2'')^4(f)^1$ configurations involving the nonbonding $f_{\pm3}$ and $f_{\pm1}$ orbitals. The next two states, $1^2E_2''$ and $2^2E_2''$, best correspond to the $(e_2')^4(e_2'')^3(f_0)^2$ and $(e_2')^4(e_2'')^4(4e_2'')^1$ configurations, respectively. These states are close in energy, indicating that the creation of a hole in the $3e_2''$ by pairing the electron in the f_0 orbital requires about the same energy as placing the last electron in the An−Ch antibonding $4e_2''$ MO. The highest energy state shown in Figure 5, the $^2E_2'$, corresponds to the $(e_2')^3(e_2'')^4(f_0)^2$ configuration. Clearly, the production of a hole in the bonding e_2' MO requires greater energy than that for the e_2'' MO. The picture that arises from these configuration energies is satisfyingly in accord with the one-electron energy levels of the anion.

Table 2 also presents the energies for selected configurations in the isoelectronic 21e series $PaCh_2^{2-}$, UCh_2^-, $NpCh_2$, and $PuCh_2^+$. For the Pa, U, and Np systems, the ground state is the $^2A_2''$ state that corresponds to the "expected" $(e_2')^4(e_2'')^4(f_0)^1$ configuration. The configurations in which one of the e_2'' or e_2' electrons is transferred to the $f_{\pm3}$ orbital become progressively lower in energy as we proceed from Pa through Pu, again reflecting the steady drop in the An 5f orbitals. For $PuCh_2^+$ we find that the ground configuration is $(e_2')^3(e_2'')^4(f_0)^1(f_{\pm3})^1$, i.e. one in which an e_2' electron is transferred to the $f_{\pm3}$ orbitals. This situation is entirely analogous to that which we discussed above for $NpCh_2^+$. The production of holes in the ligand orbitals of $NpCh_2^+$ and $PuCh_2^+$ is reminiscent of the situation in the endohedral fullerene complexes $An@C_{28}$ (An = Pa, U).[36]

Our calculated RKS ground configurations for the $AnCh_2$ molecules and $AnCh_2^+$ cations are summarized in Table 4. We will not discuss the remainder of these configurations in detail, in part because several of them involve multiple open shells and will be subjected to large spin−orbit effects. In addition, most of the calculated configurations with a hole in the ligand-based orbitals are less than 1 eV higher in energy than the lowest energy configurations. This observation strongly suggests the necessity of including nondynamic electron correlation in the density functional calculations. The ground states of these compounds will accordingly be a mixture originating from various near-degenerate configurations,[37] which we are currently unable to handle with the computational codes used. Nevertheless, we will use these ground configurations as a starting point for the discussion of the geometries and bonding in these $AnCh_2$ systems.

***D_{7h}* vs *D_{7d}* Conformations.** Before addressing the complete optimized geometries of the $AnCh_2$ systems, it is instructive to examine the relative rotational orientation of the two C_7H_7 rings. We will use the structurally characterized anion UCh_2^- as an example to discuss the conformation problem. As in the other metallocenes,[38] the two limiting conformations, namely eclipsed (D_{7h}) and staggered (D_{7d}), are expected to be nearly degenerate. The rotational preference of the complex can depend on the electronic state. We therefore have calculated the RKS energies of nine low-lying electronic configurations of UCh_2^- under D_{7h} and D_{7d} symmetry at the LDA^{NR}, LDA^R, and BP^R levels by keeping all the geometrical parameters except the rotational angle fixed at the crystallographically determined values.[10] Because the C−H bond length is unavailable from the crystal structure, the C−H bond length for benzene,[39] 1.084 Å, has been adopted in these calculations. In addition, the Ch ligand is assumed to be planar for these rotational calculations. The relative energies are summarized in Table 3. The electron configurations that were considered can be divided into two groups: those in which the metal−ligand bonding MOs are completely filled, leaving a single unpaired electron localized on the f_0, $f_{\pm1}$, $f_{\pm3}$, d_0, and $f_{\pm2}$ orbitals of the central metal, and those that have a hole in one of the frontier metal−ligand bonding MOs (e_2' or e_2'' in D_{7h}; e_{2g} or e_{2u} in D_{7h}).

The results in Table 3 reveal that, regardless of the level of calculation and the choice of electron configuration, the staggered D_{7d} conformation is lower in energy than the eclipsed

(36) It has been shown by spin−orbit CI calculations that the ground states of $An@C_{28}$ possess $(\pi^*)^1(f)^{n-1}$ configurations rather than $(f)^n$ configurations for Pa and U. See ref 7c and: Zhao, K.; Pitzer, R. M. *J. Phys. Chem.* **1996**, *100*, 4798.

(37) For an approach to the near-degenerate problem in density functional methods, see: (a) Dunlap, B. I. In *Ab initio Methods in Quantum Chemistry II*; Lawley, K. P., Ed.; Wiley: New York, 1987. (b) Wang, S. G.; Schwarz, W. H. E. *J. Chem. Phys.* **1996**, *105*, 4641 and references cited therein.

(38) (a) Bohn, R. K.; Haaland, A. *J. Organomet. Chem.* **1966**, *5*, 470. (b) Haaland, A. *Acc. Chem. Res.* **1979**, *12*, 415.

(39) Weast, R. C.; Lide, D. R.; Astle, M. J.; Beyer, W. H., Eds.; *CRC Handbook of Chemistry and Physics*, 70th ed.; CRC Press, Inc.: Boca Raton, FL, 1989; F-188.

Table 4. Restricted BP^R Energies (eV) for the Low-Energy Outer Electron Configurations of Neutral $AnCh_2$ and Cationic $AnCh_2^+$ Complexes

molecule	configuration	energy	cation	configuration	energy
$ThCh_2$	$(e_2')^4(e_2'')^2$	−174.648	$ThCh_2^+$	$(e_2')^4(e_2'')^1$	−168.497
$PaCh_2$	$(e_2')^4(e_2'')^3$	−176.711	$PaCh_2^+$	$(e_2')^4(e_2'')^2$	−170.028
UCh_2	$(e_2')^4(e_2'')^4$	−176.806	UCh_2^+	$(e_2')^4(e_2'')^3$	−169.669
$NpCh_2$	$(e_2')^4(e_2'')^4(f_0)^1$	−176.290	$NpCh_2^+$	$(e_2')^3(e_2'')^4(f_0)^1$	−169.273
	$(e_2')^4(e_2'')^3(f_0)^1(f_{\pm3})^1$	−175.436		$(e_2')^4(e_2'')^4$	−169.141
	$(e_2')^3(e_2'')^4(f_0)^1(f_{\pm3})^1$	−175.289		$(e_2')^4(e_2'')^3(f_0)^1$	−168.992
$PuCh_2$	$(e_2')^4(e_2'')^4(f_0)^1(f_{\pm3})^1$	−174.625	$PuCh_2^+$	$(e_2')^3(e_2'')^4(f_0)^1(f_{\pm3})^1$	−167.750
	$(e_2')^4(e_2'')^4(f_0)^2$	−174.616		$(e_2')^3(e_2'')^4(f_0)^2$	−167.680
	$(e_2')^4(e_2'')^3(f_0)^2(f_{\pm3})^1$	−174.322		$(e_2')^4(e_2'')^4(f_0)^1$	−167.439
	$(e_2')^3(e_2'')^4(f_0)^2(f_{\pm3})^1$	−174.310		$(e_2')^4(e_2'')^3(f_0)^1(f_{\pm3})^1$	−167.200
	$(e_2')^3(e_2'')^4(f_0)^1(f_{\pm3})^2$	−173.380		$(e_2')^4(e_2'')^3(f_0)^2$	−167.147
	$(e_2')^4(e_2'')^3(f_0)^1(f_{\pm3})^2$	−173.332			
$AmCh_2$	$(e_2')^4(e_2'')^4(f_0)^2(f_{\pm3})^1$	−174.050	$AmCh_2^+$	$(e_2')^3(e_2'')^4(f_0)^2(f_{\pm3})^1$	−167.235
	$(e_2')^4(e_2'')^4(f_0)^1(f_{\pm3})^2$	−172.957		$(e_2')^4(e_2'')^3(f_0)^2(f_{\pm3})^1$	−166.450
	$(e_2')^3(e_2'')^4(f_0)^2(f_{\pm3})^1(f_{\pm1})^1$	−172.613		$(e_2')^4(e_2'')^3(f_0)^1(f_{\pm3})^2$	−166.413
	$(e_2')^3(e_2'')^4(f_0)^1(f_{\pm3})^2(f_{\pm1})^1$	−172.538		$(e_2')^4(e_2'')^4(f_0)^1(f_{\pm3})^1$	−166.227
	$(e_2')^4(e_2'')^3(f_0)^2(f_{\pm3})^1(f_{\pm1})^1$	−172.537		$(e_2')^3(e_2'')^4(f_0)^1(f_{\pm3})^2$	−166.184
	$(e_2')^4(e_2'')^3(f_0)^1(f_{\pm3})^2(f_{\pm1})^1$	−172.413		$(e_2')^4(e_2'')^4(f_0)^2$	−166.167

D_{7h} conformation. The energy difference between the two conformations (0.5 to 1.0 kcal/mol based on the BP^R results) is remarkably invariant to the choice of electron configuration, suggesting that the energy difference is largely due to steric interactions between the two Ch rings. Because the calculated energy difference between the rotamers is very small, regardless of configuration, it is expected that the complex would exhibit virtually free rotation of the Ch rings at ambient temperatures.

These results are in agreement with the staggered geometry of this anion observed in the crystal structure,[10] although a lower C_{2h} symmetry was found in the solid state, which is likely due to crystalline packing forces. Moreover, the calculated ground-state rotation barrier of ca. 0.6 kcal/mol is similar to that observed for other sandwich compounds.[40] Although the calculated barrier is small relative to the total energies of the systems, we believe it to be reliable because of the structural similarity of eclipsed and staggered rotamers. To check the validity of the current DFT method in assessing rotation potential barriers for cyclopolyene and cyclopolyenyl sandwich compounds, we have also calculated the energies of the eclipsed and staggered conformers of $Ni(C_4H_4)_2$, $Fe(C_5H_5)_2$, $Cr(C_6H_6)_2$, and $U(C_8H_8)_2$. We find that the D_{nh} conformers are more stable than the D_{nd} ones by 0.85, 0.60, and 0.19 kcal/mol for $n = 5$, 6, and 8 at the BP^R level,[41] in good accord with the experimental findings.[42−44] On the other hand, the staggered conformer for $Ni(C_4H_4)_2$ is found to be 0.16 kcal/mol more stable than the eclipsed one, as we have found for UCh_2^-. We therefore have good confidence in the applicability of the same method to the cycloheptatrienyl sandwich compounds.

Although the staggered conformer is the more stable one, the rotation barrier is very small. Because the D_{7h} and D_{7d} point groups are isomorphic, and because the calculations are somewhat easier to carry out in D_{7h} symmetry, all other calculations and the following discussion focus only on the conformations of D_{7h} symmetry. The bonding pictures are essentially the same for the staggered and the eclipsed conformers, although the labels of irreducible representations differ slightly.

Geometries. The prediction of reasonable geometries is one of the most common criteria used to judge the applicability of electronic structure methods. The correct calculation of the geometries of sandwich compounds has proven difficult for many methodologies. For example, the determination of the metal−carbon distance in ferrocene has been a notorious challenge for ab initio methods.[45] The calculation of the metric parameters in the $AnCh_2$ systems promises to be an even more challenging problem owing to greater dynamic and non-dynamic electron correlation effects, the presence of significant scalar and spin−orbit relativistic effects, and the need for more demanding basis sets.

Under the constraint of D_{7h} symmetry, $AnCh_2$ complexes have four geometric degrees of freedom: The An−C distance (or, equivalently, the An−X distance, where X is the centroid of the C_7 ring), the C−C distance, the C−H distance, and the ∠H−C−X angle, which indicates how much the H atoms are out of the C_7 plane. To assess the effects of electron configuration and level of theory, we have calculated the optimized geometry of UCh_2^- by using the LDA^{NR}, LDA^R, BP^R (RKS), and BP^R (UKS) approaches. The calculated metric parameters and the corresponding experimental values are listed in Table 5.

Several trends are apparent in Table 5. First, at each level of calculation, the lowest energy is achieved in the $(3e_2')^4(3e_2'')^4(5a_2'')^1$ configuration, that is, the "extra" electron occupies the U-based orbital that is predominantly $5f_0$ in character. Second, there are no significant differences between the bond lengths optimized for different configurations, except for those having a hole in the ligand-based $3e_2'$ and $3e_2''$ MOs. As discussed earlier, those MOs encompass strong U−C bonding interactions, so it is not surprising that the U−C distances lengthen when an electron is removed from them. Third, we note that the inclusion of the scalar relativistic corrections shrinks the U−C

(40) The barrier to internal rotation of the Cp rings in $FeCp_2$ is 0.9 ± 0.3 kcal/mol. See: (a) Haaland, A.; Nilsson, J. E. *Acta Chem. Scand*. **1968**, *22*, 2653. (b) Laane, J. *J. Coord. Chem*. **1971**, *1*, 75. (c) Carter, S.; Murrell, J. N. *J. Organomet. Chem*. **1980**, *192*, 399. (d) Bencivenni, L.; Ferro, D.; Pelino, M.; Teghil, R. *J. Indian Chem. Soc*. **1980**, *57*, 1062. (e) Marverick, E.; Dunitz, J. D. *Mol. Phys*. **1987**, *62*, 451.

(41) Li, J.; Bursten, B. E. Unpublished results.

(42) Although earlier X-ray experiments revealed that the D_{5d} conformer of $Fe(C_5H_5)_2$ was more stable in the solid state, the D_{5h} conformer has been found to be more stable in the gas phase by electron diffraction and in the solid state by X-ray or neutron diffraction. See: (a) Dunitz, J. D.; Orgel, L. E.; Rich, A. *Acta Crystallogr*. **1956**, *9*, 373 and references cited therein. (b) Bohn, R. K.; Haaland, A. *J. Organomet. Chem*. **1966**, *5*, 470. (c) Seiler, P.; Dunitz, J. D. *Acta Crystallogr*. **1979**, *B35*, 1068. (d) Seiler, P.; Dunitz, J. D. *Acta Crystallogr*. **1982**, *B38*, 1741. (e) Takusagawa, F.; Koetzle, T. F. *Acta Crystallogr*. **1979**, *B35*, 1074.

(43) As shown by X-ray and electron diffraction experiments, the D_{6h} conformer of $Cr(C_6H_6)_2$ is more stable in both the crystalline and gas phases. See: (a) Cotton, F. A.; Dollase, W. A.; Wood, J. S. *J. Am. Chem. Soc*. **1963**, *85*, 1543. (b) Haaland, A. *Acta Chem Scand*. **1965**, *19*, 41. (c) Keullen, E.; Jellinck, F. *J. Organomet. Chem*. **1966**, *5*, 490. (d) Schaefer, L.; Southern, J. F.; Cyvin, S. J.; Brunvoll, J. *J. Organomet. Chem*. **1970**, *24*, 913.

(44) In the solid state, the D_{8h} conformer of $U(C_8H_8)_2$ is found to be more stable: (a) Zalkin, A.; Raymond, K. N. *J. Am. Chem. Soc*. **1969**, *91*, 5667. (b) Avdeef, A.; Raymond, K. N.; Hodgson, K. O.; Zalkin, A. *Inorg. Chem*. **1972**, *11*, 1083.

(45) (a) Park, C.; Almlöf, J. *J. Chem. Phys*. **1991**, *95*, 1829. (b) Pierloot, K.; Persson, B. J.; Roos, B. O. *J. Phys. Chem*. **1995**, *99*, 3465. (c) Koch, H.; Jørgensen, P.; Helgaker, T. *J. Chem. Phys*. **1996**, *104*, 9528.

Table 5. Restricted LDA^{NR}, LDA^{R}, and BP^{R} and Unrestricted BP^{R} Optimized Bond Distances (Å), Angles (deg), and Corresponding Energies (eV) for Several Low-Lying Outer Electron Configurations of UCh_2^- in Its Eclipsed (D_{7h}) Conformation

configuration	U−X[a]	U−C	C−C	C−H	∠HCX[a]	*E*
			LDA^{NR} (RKS)			
$(e_2')^4(e_2'')^4(f_0)^1$	2.173	2.717	1.416	1.098	177.2	−195.093
$(e_2')^4(e_2'')^4(f_{\pm1})^1$	2.181	2.725	1.417	1.097	177.7	−194.601
$(e_2')^4(e_2'')^4(f_{\pm3})^1$	2.172	2.718	1.418	1.097	176.9	−194.564
$(e_2')^4(e_2'')^3(f_0)^1(f_{\pm3})^1$	2.225	2.759	1.416	1.098	178.2	−194.450
$(e_2')^3(e_2'')^4(f_0)^1(f_{\pm3})^1$	2.244	2.774	1.415	1.098	178.0	−194.467
			LDA^{R} (RKS)			
$(e_2')^4(e_2'')^4(f_0)^1$	2.002	2.586	1.420	1.098	175.1	−194.353
$(e_2')^4(e_2'')^4(f_{\pm1})^1$	2.008	2.592	1.423	1.097	176.0	−193.938
$(e_2')^4(e_2'')^4(f_{\pm3})^1$	1.991	2.580	1.424	1.097	174.8	−193.904
$(e_2')^4(e_2'')^3(f_0)^1(f_{\pm3})^1$	2.045	2.620	1.422	1.098	176.9	−192.576
$(e_2')^3(e_2'')^4(f_0)^1(f_{\pm3})^1$	2.066	2.637	1.421	1.098	176.6	−191.970
			BP^{R} (RKS)			
$(e_2')^4(e_2'')^4(f_0)^1$	2.051	2.634	1.434	1.095	176.0	−178.380
$(e_2')^4(e_2'')^3(f_0)^1(f_{\pm3})^1$	2.105	2.677	1.435	1.095	177.6	−176.709
$(e_2')^3(e_2'')^4(f_0)^1(f_{\pm3})^1$	2.128	2.695	1.435	1.095	177.5	−176.178
			BP^{R} (UKS)			
$(e_2')^4(e_2'')^4(f_0)^1$	2.054	2.636	1.434	1.094	176.0	−178.729
$(e_2')^4(e_2'')^3(f_0)^1(f_{\pm3})^1$	2.114	2.684	1.435	1.094	177.6	−177.557
$(e_2')^3(e_2'')^4(f_0)^1(f_{\pm3})^1$	2.134	2.699	1.435	1.095	177.3	−176.994
			Experimental[b]			
	1.98(2)	2.53(2)	1.37(7)	[1.084]		

[a] X represents the centroid of the C_7 ring. [b] From ref 10. Values in parentheses are crystallographic esd's. Value in brackets is assumed.

distances by more than 0.1 Å. This observation reflects the fact that relativity has reduced the kinetic energy of the bonding electrons,[46] thereby strengthening the U−Ch bonding and shortening the U−Ch distances. In addition, the semicore 6s and 6p orbitals are radially contracted and significantly lowered in energy upon the inclusion of relativistic effects. The Pauli repulsions between the uranium semicore electrons and the core electrons of the carbon atoms in C_7H_7 rings are accordingly reduced, which also serves to reduce the U−C distances. Finally, the U−C bond lengths optimized with the gradient-corrected exchange functionals (BP^{R}) are all ca. 0.05 Å longer than the corresponding LDA^{R} distances.

The results in Table 5 are consistent with previous DFT studies of the geometries of molecules. It has been found that, for lighter molecules, various density functional approaches usually overestimate bond lengths by 0.02−0.04 Å, especially with the gradient-corrected exchange functionals.[47,48] For heavier molecules, however, LDA^{R} calculations on some lanthanide oxide compounds indicate that the bond distances are underestimated by 0.05 Å, whereas the calculations including Becke's exchange correction result in an expansion of bond lengths,[49] as noted above. We also note that the bond distances and angle optimized by BP^{R} (RKS) and BP^{R} (UKS) methods are virtually the same, implying that the spin-polarization effect on the geometry is probably negligible. The U−C distances optimized by using the LDA^{R}, BP^{R} (RKS), and BP^{R} (UKS) approaches are all somewhat longer than the crystallographic value. This discrepancy can be attributed to several factors, including the effects of crystal packing and the counterions in the crystal,[50] as well as the omission of spin−orbit coupling, non-dynamic electron correlation, and high angular momentum polarization functions in the basis sets during the geometry optimizations. Although the calculated bond distances deviate slightly from the experimental ones, we expect that comparative calculations across a series of systems will provide meaningful trends in the changes in bond distances. These calculations have been carried out predominantly at the BP^{R} level of calculation.

We have optimized the geometries at the BP^{R} level for the ground states of $AnCh_2^q$ compounds (An = Th−Am; $q = 2-$, $1-$, 0, $1+$); a complete listing of the calculated geometries is available in the Supporting Information. For the most part, the geometries vary little as the charge is changed; apparently the addition or removal of an electron has only subtle effects on the overall geometries of the complexes. There is a general, albeit not monotonic, decrease in An−C bond length with increasing atomic number, which is a manifestation of the so-called "actinide contraction".[51] Recall that the U−C bond length optimized at the BP^{R} level is about 0.1 Å longer than the crystalline experimental bond lengths for UCh_2^-. If we assume that the same deviation occurs for the other Ch sandwich compounds, we predict the experimental Th−C and Pa−C distances to be 2.66 and 2.55 Å, while the U−C, Np−C, Pu−C, and Am−C distances should all be ca. 2.53 Å.

In all of the optimized structures, the H atoms are tipped slightly out of the C_7 plane, a phenomenon also observed for ferrocene. Neutron diffraction experiments indicate that the H atoms in the C_5H_5 ring of $FeCp_2$ are bent out of the carbon ring plane toward the metal by 1.6° ± 0.4.[42e,52] In our BP^{R} geometry optimizations, the C−H bonds in the UCh_2^- and $FeCp_2$ molecules are found to be bent by about 4° and 0.7°, respectively, toward the metal atom. The larger C−H bending angle for UCh_2^- than for $FeCp_2$ is in line with the previous theoretical prediction by Hoffmann et al.[53] In general, the tip angle decreases as the overall charge on the $AnCh_2^q$ complexes becomes more positive.

The source of the tipping of the H atoms toward the An center in $AnCh_2^q$ systems is analogous to that for the 3d metallocenes: The tipping causes a slight reorientation of the pπ orbitals toward the central metal, which leads to increased An−Ch interaction. For UCh_2^-, for example, the tipping leads to a 1.9-kcal/mol increase in the An−Ch bonding energy relative to a constrained planar C_7H_7 ring.

The C−C bond lengths in Tables 5 and 6 provide us with interesting information regarding the metal−ligand bonding in $AnCh_2^q$ complexes. Both ligand-to-metal donation from the bonding π_1 MO of Ch and metal-to-ligand back-donation into the antibonding π_2 MO of Ch will serve to lengthen the C−C bonds. In Table 5 we see that the relativistic C−C bonds are less than 0.01 Å longer than the non-relativistic ones, which is consistent with the relativistically shortened An−C distances. Overall, the C−C bond lengths are far less sensitive to the inclusion of relativistic effects than are the An−C bond lengths,

(46) Ziegler, T.; Snijders, J. G.; Baerends, E. J. In *The Challenge of d and f Electrons: Theory and Computation*; Salahub, D. R., Zerner, M. C., Eds.; American Chemical Society: Washington, DC, 1989. The relativistic contraction of bond distances has also been rationalized in terms of the attractive Hellmann−Feynman force arising from the relativistic change in electron density: Schwarz, W. H. E.; Chu, S. Y.; Mark, F. *Mol. Phys.* **1983**, *50*, 603.

(47) Johnson, B. G.; Gill, P. M. W.; Pople, J. A. *J. Chem Phys*. **1993**, *98*, 5612.

(48) Handy, N. C. In *Lecture Notes in Quantum Chemistry II*; Roos, B. O., Ed.; Springer-Verlag: Berlin, 1994.

(49) Wang, S. G.; Pan, D. K.; Schwarz, W. H. E. *J. Chem. Phys*. **1995**, *102*, 9296.

(50) The Madelung potentials of the crystal field could have a considerable influence on the bond lengths of charged molecules. See, for example: Li, J.; Irle, S.; Schwarz, W. H. E. *Inorg. Chem.* **1996**, *36*, 100.

(51) (a) See, for example: Huheey, J. E.; Keiter, E. A.; Keiter, R. L. *Inorganic Chemistry: Principles of Structure and Reactivity*, 4th ed.; Harper Collins: New York, 1993; Chapter 14. (b) For a recent theoretical analysis of actinide contraction and its comparison with the lanthanide contraction, see: Seth, M.; Dolg, M.; Fulde, P.; Schwerdtfeger, P. *J. Am. Chem. Soc*. **1995**, *117*, 6597 and references therein.

(52) An electron diffraction experiment produces a bigger bent angle, 3.7(9)°: Haaland, A.; Lusztyk, J.; Novak, D. P.; Brunvoll, J.; Starowieyski, K. B. *J. Chem. Soc., Chem. Commun*. **1974**, *54*.

(53) Elian, M.; Chen, M. M. L.; Mingos, M. P.; Hoffmann, R. *Inorg. Chem*. **1976**, *15*, 1148.

Table 6. The First Adiabatic Ionization Energies (eV) for $AnCh_2^q$ (An = Th−Am; $q = 2-, 1-, 0$) and the Transition-State Ionization Energies (in parentheses) for Neutral $AnCh_2$ Molecules[a]

q	Th	Pa	U	Np	Pu	Am
2−	−2.16	−3.90	−3.68	−3.89	−3.10	−2.92
1−	1.96	2.33	1.57	1.66	2.29	0.98
0	6.15 (6.15)	6.68 (6.63)	7.14 (7.09)	7.02 (7.00)	6.87 (6.80)	6.81 (6.75)

[a] Calculations at the restricted BP^R level.

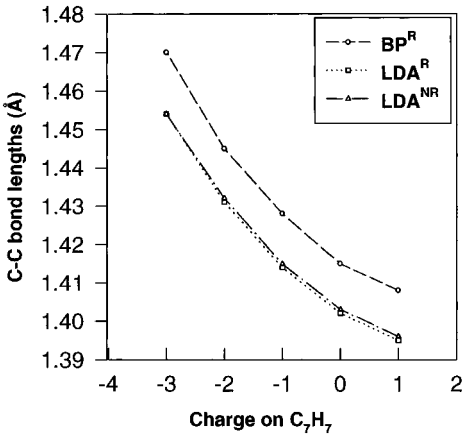

Figure 6. Optimized LDA^{NR}, LDA^R, and BP^R C−C bond lengths plotted vs the charge q of $C_7H_7^q$.

indicating, as expected, that the relativistic effects have negligible direct effect on the geometry of the C_7H_7 rings.

In general, the C−C bond lengths increase monotonically as q becomes more negative. This observation is not surprising; it indicates that a fraction of each added electron is "shuttled" into the antibonding π_2 MOs of the Ch ligands. Thus, the C−C bond lengths provide an indication of the formal charges on the Ch ligands in the complexes. To provide this comparison, we have calculated the C−C distances in the free $C_7H_7^q$ ligand ($q = 3-, 2-, 1-, 0, 1+$), corresponding to variation of the π_2 population from 4 to 0. In Figure 6, the optimized LDA^{NR}, LDA^R, and BP^R C−C bond lengths are plotted versus the charge q for the $C_7H_7^q$ ligands. As expected, the C−C bond lengths increase (by 0.01−0.02 Å) as each electron is added. The C−C distances from BP^R calculations are systematically 0.012 Å longer than those from LDA^R calculations, while the C−C distances are practically the same from LDA^{NR} and LDA^R calculations. The relation between the C−C distances d(C−C), calculated at the LDA^R and BP^R levels for free $C_7H_7^q$, and the charge (q) can be well reproduced by the quadratic functions in eqs 1 and 2:

$$d(\mathrm{C-C})_{\mathrm{LDA}} = 1.402 - 0.009414q + 0.002643q^2 \quad (1)$$

$$d(\mathrm{C-C})_{\mathrm{BP}} = 1.415 - 0.009686q + 0.002857q^2 \quad (2)$$

A comparison of these free ligand C−C bond distances to those in the $AnCh_2^q$ complexes (LDA^R: 1.41−1.43 Å; BP^R: 1.43−1.45 Å) indicates that the Ch ligands in the complexes have formal charges in the range $q = 1-$ to $2-$. We will see that these values are in good agreement with the formal oxidation states assigned via population analysis, which we will discuss in the next section.

Quantitative Aspects of the Bonding in $AnCh_2$ Complexes. In light of our results on the configurations, conformations, and geometries of the $AnCh_2$ compounds, we will now address some of the quantitative aspects of the bonding in these cycloheptatrienyl sandwich compounds. By comparing the energy level diagram of UCh_2 (Figure 4) with that of $U(COT)_2$, which has been previously analyzed in detail,[8] we can expect that the bonding in these two molecules should be somewhat similar. However, due to the weak antibonding nature of the frontier π_2 orbitals of the C_7H_7 ring, there will be some noticeable differences as well.

We will first return to the spin−orbit averaged energy levels for UCh_2, presented in Figure 4. As noted before, the uranium AO energies are greatly affected by relativistic effects. Upon the inclusion of the scalar relativistic effects, the U 6s and 7s orbitals are stabilized by 12.29 and 0.77 eV, respectively, due to the relativistic mass−velocity effect (direct relativistic effect).[54] The U 5f and 6d orbitals are destabilized by 6.57 and 1.57 eV, primarily because of the increased electronic shielding caused by the contraction of s-type orbitals (indirect relativistic effect).[55] The 6p orbitals are stabilized by 0.83 eV, but the 7p orbitals are actually slightly destabilized by 0.30 eV.[56] These changes in the U AO energies caused by relativity have profound effects on the interaction of the U AOs with the C_7H_7 orbitals.

Our calculations on UCh_2 have treated the U 6s and 6p AOs (which are considered "semicore" orbitals) as variational orbitals. Although it is generally regarded that the U 6s and 6p semicore orbitals should be included in calculations of actinide complexes, the roles played by these orbitals in the bonding and geometries of some uranium compounds have been the subject of some controversy.[57,58] In the present calculation, we see very little interaction between the U 6s orbital and the ligands; the principal interactions between the ligands and the U s orbitals involve the high-lying U 7s AO. As an example, the $4a_1'$ MO of UCh_2, which is the lowest one shown in Figure 4, contains 0% U 6s and 13% U 7s character. The 6p orbitals interact more significantly with the ligand-based orbitals than does the 6s. For example, the $1a_2''$ MO, which is largely U $6p_0$ in character, contains ca. 40% contribution from C-based AOs. The interaction of the $6p_{\pm1}$ orbitals is relatively less because of the disadvantageous angular orientation of these orbitals with respect to the C_7H_7 rings.

Of course, the most important frontier orbitals of UCh_2 are those generated by interaction of the uranium 5f and 6d orbitals with the pπ orbitals of the Ch rings (Figure 3). The energies of these MOs reflect the differing degrees of interaction between the metal and ring orbitals. For example, the primarily Ch-based $3e_1''$ and $4e_1'$ MOs show an energy reversal relative to the $(Ch)_2$ π_1' and π_1'' group orbitals. The π_1' and π_1'' group orbitals interact primarily with the U $5f_{\pm1}$ and $6d_{\pm1}$ AOs, respectively. The 6d orbitals are more radially diffuse than are

(54) The mass−velocity effect for s-type orbitals is partially cancelled by the Darwin effects. See, for example: Schwarz, W. H. E. In *Theoretical Models of Chemical Bonding*; Maksić, Z., Ed.; Springer: Berlin, 1990; p 595.

(55) For qualitative and quantitative discussions of direct and indirect relativistic effects, see, for example: (a) Pitzer, K. S. *Acc. Chem. Res*. **1979**, *12*, 271. (b) Pyykkö, P.; Desclaux, J.-P. *Acc. Chem. Res*. **1979**, *12*, 276. (c) Pyykkö, P. *Chem. Rev*. **1988**, *88*, 563. (d) Schwarz, W. H. E.; van Wezenbeek, E. M.; Baerends, E. J.; Snijders, J. G. *J. Phys*. **1989**, *B22*, 1515.

(56) For a discussion of the effects of mass−velocity, Darwin, and spin−orbit coupling on p-type orbitals, see, for example: Wang, S. G.; Schwarz, W. H. E. *J. Mol. Struct. (Theochem)* **1995**, *338*, 347.

(57) (a) Tatsumi, K.; Hoffmann, R. *Inorg. Chem*. **1980**, *19*, 2656. (b) Pyykkö, P.; Lohr, L. L., Jr. *Inorg. Chem*. **1981**, *20*, 1950. (c) Pyykkö, P.; Jové, J. *New J. Chem*. **1991**, *15*, 717.

(58) Wadt, W. R. *J. Am. Chem. Soc*. **1981**, *103*, 6053.

the 5f AOs,[59] and the angular distribution of the $6d_{\pm1}$ orbitals is ideally suited to interact with the π_1'' group orbital. As a consequence, we find a much greater contribution of the $6d_{\pm1}$ AOs to the $3e_1''$ MO (15%) than of the $5f_{\pm1}$ AOs to the $4e_1'$ MO (1%).

The most important interactions between U and $(Ch)_2$ involve the $5f_{\pm2}-\pi_2''$ and $6d_{\pm2}-\pi_2'$ pairs (Figure 4). The relative energetic ordering of the lower-energy, ligand-based e_2' and e_2'' MOs will be a compromise of (i) the initial energetic difference of the $(Ch)_2$ π_2' and π_2'' group orbitals, (ii) the better energetic match between the U $5f_{\pm2}$ and the ligand π_2'' orbital, and (iii) the greater radial extension of the $6d_{\pm2}$ AOs relative to the $5f_{\pm2}$ AOs. The ordering of similar MOs in $U(COT)_2$ was the subject of some controversy and has been resolved experimentally by Green et al. via variable-energy photoelectron spectroscopy.[60] For UCh_2, we find that the $3e_2'$ MO, which has U 6d character, is 0.4 eV lower in energy than the $3e_2''$ MO, which has U 5f character. This MO ordering is analogous to that in the corresponding e_{2g} and e_{2u} MOs of $U(COT)_2$ inasmuch as the MO with U 6d character is lower in energy than the one with U 5f character.

Although the $3e_2'$ MO is lower in energy than the $3e_2''$ MO, we find that the interaction of the $5f_{\pm2}$ AOs with the π_2'' group orbitals is as strong as that of the $6d_{\pm2}$ AOs and the π_2' $(Ch)_2$ orbitals, largely because of the close energetic match of the $5f_{\pm2}$ and π_2'' orbitals; in fact, as is evident in Figure 4, these orbitals are nearly isoenergetic ($\Delta E = 0.64$ eV), which should lead to MOs that are nearly equal U and Ch_2 in character. Upon coordination to the U atom, the π_2'' and π_2' group orbitals of Ch_2 are stabilized by the $5f_{\pm2}$ and $6d_{\pm2}$ orbitals by 1.71 and 1.49 eV, respectively, showing the $5f_{\pm2}-\pi_2''$ interaction energy is larger than the $6d_{\pm2}-\pi_2'$ interaction. In addition, the angular distribution of the $5f_{\pm2}$ orbitals is directed toward the two C_7H_7 rings, whereas the $6d_{\pm2}$ orbitals lie mainly in the σ_h plane through the U atom. Therefore, the $5f_{\pm2}$ AOs are more efficient with respect to angular overlap even though they are more radially contracted than the 6d AOs. As a consequence of these effects, the contribution of the U $5f_{\pm2}$ orbitals to the $3e_2''$ orbitals is 54%, but that of the $6d_{\pm2}$ orbitals to the $3e_2'$ orbitals is only 29%. As noted earlier, in the $^1A_1'$ closed-shell state of UCh_2 the $3e_2'$ and $3e_2''$ MOs are completely filled, and the $3e_2''$ is the HOMO of the molecule.

Immediately above the $3e_2'$ and $3e_2''$ MOs is a manifold of largely U 5f-based MOs, namely the $5a_2''$ (96% $5f_0$), $3e_3'$ (97% $5f_{\pm3}$), and $5e_1'$ (92% $5f_{\pm1}$) MOs. These MOs, which comprise five of the seven U 5f AOs, lie in a narrow energetic band (ca. 0.5 eV). The remaining two 5f orbitals are the $5f_{\pm2}$ AOs, which are involved in the strong interaction with the $(Ch)_2$ π_2'' orbitals. Thus, the $4e_2''$ MO (46% $5f_{\pm2}$), which is the antibonding counterpart of the bonding $3e_2''$ MO discussed above, is greatly destabilized relative to the other 5f-based MOs. We have observed this ligand-induced "splitting out" of one or more 5f orbitals in other organoactinide complexes, such as Cp_3An systems.[61]

Other $AnCh_2^q$ complexes of the early actinides are expected to have bonding interactions similar to those in UCh_2, although they will differ quantitatively because of the variations in the 6d and 5f orbital energies. A further complication in determining the electronic structures of these complexes arises because of inevitable violations of the aufbau principle, which should always be followed in any density functional approach.[62] In DFT methods, the orbital energies of virtual orbitals tend to be too low as compared to those of the occupied ones.[63] Thus, apparent violations of the aufbau principle often arise when the frontier orbitals are closely spaced in energy and are not completely filled. In the case of UCh_2^-, for instance, placing the added electron in the f_0 orbital causes the unoccupied $f_{\pm3}$ orbitals to lie below the f_0 orbital. Conversely, if the electron is put in the $f_{\pm3}$ orbitals, then the unoccupied f_0 orbital lies below the $f_{\pm3}$ orbitals.

To avoid these difficulties, we have used an approximation in which the electron density is "smeared out" among closely spaced orbitals near the HOMO. In this procedure, frontier orbitals near the HOMO (within 0.05 hartree) are optimized with fractional occupations, which greatly improves the SCF convergence. The geometries for all the $AnCh_2$ complexes have been reoptimized within this approximation. The calculated fractional orbital occupations and energies for the frontier MOs of the neutral $AnCh_2$ molecules (An = Th−Am) are displayed in Figures 7 and 8. In Figure 8, the percentage contributions of the $6d_{\pm2}$ and $5f_{\pm2}$ AOs to the $3e_2'$ and $3e_2''$ MOs are indicated.

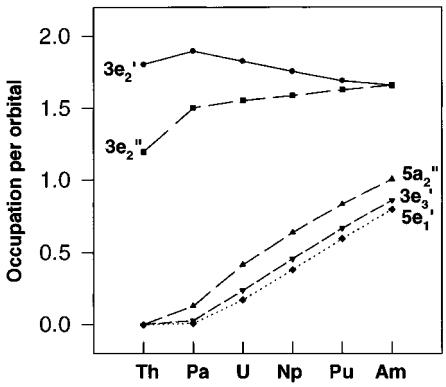

Figure 7. Calculated fractional orbital occupations for the frontier MOs of the neutral $AnCh_2$ molecules (An = Th−Am).

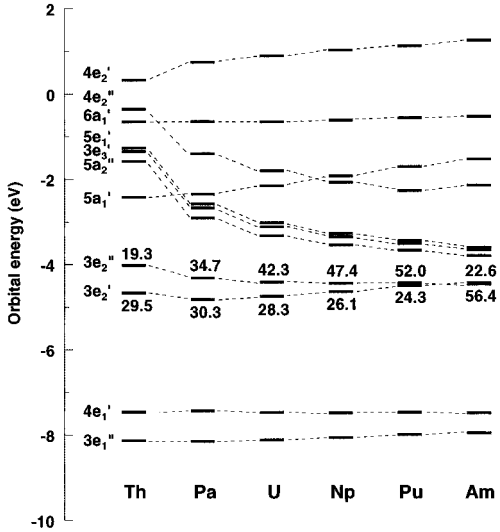

Figure 8. Energies of the frontier MOs of the neutral $AnCh_2$ molecules (An = Th−Am) and the percentage contributions of the $6d_{\pm2}$ and $5f_{\pm2}$ AOs to the $3e_2'$ and $3e_2''$ MOs.

(59) A numerical relativistic Dirac−Fock calculation for the uranium atom indicates that the spin−orbit averaged radii of the maximum radial density are 0.86, 0.56, and 1.30 Å for the 6p, 5f, and 6d orbitals, respectively: Desclaux, J. P. *At. Data Nucl. Data Tables* **1973**, *12*, 311.

(60) Brennan, J. G.; Green, J. C.; Redfern, C. M. *J. Am. Chem. Soc.* **1989**, *111*, 2373.

(61) See, for example: Bursten, B. E.; Rhodes, L. F.; Strittmatter, R. J. *J. Am. Chem. Soc.* **1989**, *111*, 2758.

(62) Janak, J. F. *Phys. Rev.* **1978**, *B18*, 7165.

(63) Unlike the Hartree−Fock method, in which virtual orbitals are artificially destabilized, in DFT methods, the Kohn−Sham virtual orbitals are generally "too low" in energy, and the addition of an electron to a molecular orbital tends to increase its energy. See: (a) Cook, D. B. *Int. J. Quantum Chem.* **1996**, *60*, 793. (b) Slater, J. C.; Mann, J. B.; Wilson, T. M.; Wood, J. H. *Phys. Rev.* **1969**, *184*, 672. (c) Slater, J. C. *Quantum Theory for Molecules and Solids. The Self-Consistent Field for Molecules and Solids*; McGraw-Hill: New York, 1974; Vol. 4.

Figures 7 and 8 show regular periodic trends in the orbital structure of $AnCh_2$ as one proceeds from Th to Am. $ThCh_2$ is, in essence, electron deficient; there are not enough electrons to fill the ligand-based $3e_2''$ and $3e_2'$ orbitals, and the occupations of these orbitals are clearly smaller in $ThCh_2$ than in $PaCh_2$. The LUMO of $ThCh_2$ is the 6d/7s-based $5a_1'$ MO; as we have seen previously for organothorium complexes, the 6d orbitals are lower in energy than the 5f orbitals.[64] As we proceed through the actinide series, the 5f AOs drop in energy while the 6d AOs rise slightly. Thus, the largely nonbonding 5f-based MOs ($5a_2''$, $3e_3'$, and $5e_1'$) show a steady drop in energy with increasing nuclear charge, and as the number of electrons increases, their fractional occupations increase regularly. Further, as noted in Figure 8, the An 5f contribution to the $3e_2''$ MO increases monotonically as the energy of the 5f orbitals drops. The energy of the 5f-based $4e_2''$ MO, which is the An−Ch antibonding counterpart of the $3e_2''$ MO, largely parallels those of the other 5f-based MOs.

The fact that the An 5f contribution to the $3e_2''$ MOs increases as we progress from Th to Am does not necessarily indicate an increasing interaction between the $5f_{\pm 2}$ AOs and the Ch π_2 orbitals. In fact, the energies of the $3e_2''$ orbitals are nearly constant through the series while the $4e_2''-3e_2''$ energy gap decreases, indicating a *decrease* in the bonding and antibonding interactions between the An and ring orbitals. These seemingly contradictory observations reflect the fact that although the 5f orbitals become closer in energy to the Ch π_2 from Th to Am, the 5f orbitals are simultaneously becoming more and more radially contracted. This "actinide contraction" results in a net reduction of orbital overlap.[65] These two counteracting factors, decreasing 5f orbital energy and decreasing 5f radial extension, nearly cancel one another, giving rise to a net decrease in the role of the 5f orbitals in the bonding of these compounds. We have previously noted these periodic effects in Cp_3An (An = U−Cf) compounds.[66] We will soon show that the calculated An to C_7H_7 bond strengths also show this decreasing 5f participation as we proceed from left to right.

An−C_7H_7 Bond Energies and Ionization Energies. We can use the optimized geometries and the theoretically determined ground configurations to examine trends in the bond energies, ionization energies, and electron affinities of the $AnCh_2$ complexes. For the neutral compounds, we have calculated the *homolytic* bond energies, D_e(homo), defined here as:

$$D_e(\text{homo}) = {}^1/_2\{E[\text{An}] + 2E[C_7H_7] - E[\text{An}(C_7H_7)_2]\} \quad (3)$$

E[An] is the average-of-configuration energy of the actinide atom, calculated in the atomic ground configuration with spin-polarization corrections. $E[C_7H_7]$ is the molecular energy of a neutral D_{7h} C_7H_7 ligand in the π electron configuration $(a_2'')^2(e_1'')^4(e_2'')^1$ ($^2E_2''$ state). These calculations were carried out at both the UKS and RKS levels, with very similar results. We report the UKS results here.

Figure 9 shows a plot of D_e(homo) vs An for the neutral $AnCh_2$ molecules. The decrease in the bond energies from $PaCh_2$ to $AmCh_2$ is in accord with the bonding picture presented earlier for $AnCh_2$ complexes. As noted, the 5f orbitals contract with increasing atomic number, which leads to a decrease in the overlap between the actinide $5f_{\pm 2}$ AOs and the e_2'' ring orbitals. In addition, the An 6d−Ch π_2 energy gap continually increases with increasing atomic number, which leads to decreased interaction between the An 6d AOs and the e_2' ring orbitals. The decrease in D_e(homo) from Th to Am suggests that the stabilities of $AnCh_2$ sandwich compounds will decrease accordingly.[67,68]

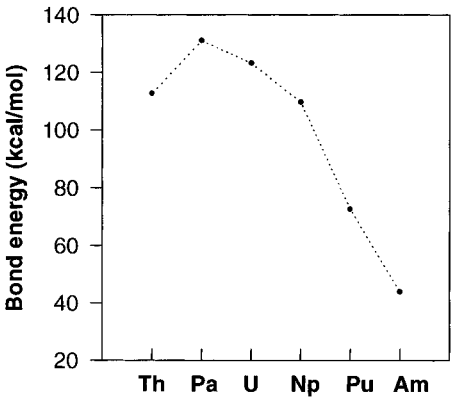

Figure 9. Plot of the homolytic bond energy [D_e(homo)] vs An for the neutral $AnCh_2$ molecules.

We have also used the ground electron configurations to calculate the adiabatic first ionization energy (IE_1) and the adiabatic electron affinity (EA) for the $AnCh_2^q$ complexes. These quantities are defined as

$$IE_1 = E(AnCh_2^+, R_e^+) - E(AnCh_2, R_e) \quad (4)$$

$$EA = -[E(AnCh_2^-, R_e^-) - E(AnCh_2, R_e)] \quad (5)$$

where $E(AnCh_2^q, R_e^q)$ is the total energy of the molecule or ion at its optimized geometry. It is evident that the EA of $AnCh_2$ is equal to the adiabatic first IE of $AnCh_2^-$. Therefore, our discussion will focus on the trends in the values of IE_1 for the neutral and anionic species. Because the geometries change little upon the addition or removal of an electron, the adiabatic IEs will be very close in value to the vertical IEs.

The adiabatic IE_1 values for the $AnCh_2$ and $AnCh_2^-$ complexes are listed in Table 6. We also list the values for the neutral $AnCh_2$ molecules obtained by using Slater's transition state (TS) method.[69] Several trends are apparent. First, the values of IE_1 show a general increase as from Th to Pa to U, and decrease from that point on. This observation is consistent with the bond energy analysis, which follows the same trends (Figure 9). Second, the ionization energies calculated by the TS method are generally in excellent agreement with those calculated by total energy differences. Third, the ionization energies of the anions are all positive, which implies that the EA values of the neutrals are all positive. Thus, the $AnCh_2^-$ anions are bound relative to the neutral $AnCh_2$ molecule plus a free electron, at least in the gas phase. We believe that this observation explains in part why the UCh_2^- anion rather than the neutral, closed-shell UCh_2 molecule is the first $AnCh_2^q$ complex to be isolated experimentally.

(64) Bursten, B. E.; Rhodes, L. F.; Strittmatter, R. J. *J. Am. Chem. Soc.* **1989**, *111*, 2756.

(65) For $AnCh_2$ (An = Pa−Am), the orbital overlaps of $5f_{\pm 2}-e_2''$ are 0.113, 0.109, 0.093, 0.092, and 0.081, respectively, and the orbital overlaps of $6d_{\pm 2}-e_2'$ are all ca. 0.30.

(66) Strittmatter, R. J.; Bursten, B. E. *J. Am. Chem. Soc.* **1991**, *113*, 552 and references therein.

(67) Because we have assumed a constant C_7H_7 in the bond energy analysis, the bond energies are directly related to the *atomization energy*, D_e(atom), which is defined as

$$D_e(\text{atom}) = E(\text{An}) + 14E(\text{C}) + 14E(\text{H}) - E[\text{An}(C_7H_7)_2]$$

For our calculations, D_e(atom) = $2D_e$(homo) + 3082, in kcal/mol.

(68) The bond energies reported here are calculated without spin−orbit effects. As a test of the validity of this assumption, we have calculated the bond energy of UCh_2 with the inclusion of spin−orbit effects. We find that the energies of the U atom and the UCh_2 molecule are lowered by nearly the same amount. Thus, the effect of spin−orbit coupling on the calculated bond energy is small. We expect that the trend in the bond energies presented in Figure 9 would be qualitatively the same if spin−orbit effects were included.

(69) Slater, J. C. *Adv. Quantum Chem.* **1972**, *6*, 1.

We have also examined the ionization energies of the $AnCh_2^{2-}$ dianions, which will give the EA of the $AnCh_2^-$ anions. For all An, we find that $AnCh_2^-$ has a negative EA, implying that these anions will not bind an electron in the gas phase. It therefore seems unlikely that $AnCh_2^{2-}$ complexes will be found to be stable.

Formal Charges in $AnCh_2^q$ Complexes. We will return to the question of the best description of the formal charges on An and C_7H_7 in these sandwich complexes, this time via population analysis of the ground charge distributions. Earlier we used analysis of the C−C bond lengths to propose that the C_7H_7 ligands in the $AnCh_2^q$ complexes carry a formal charge that is between 1− and 2−.

Our calculated electron affinities for $C_7H_7^+$, C_7H_7, $C_7H_7^-$, and $C_7H_7^{2-}$ are 6.20, 0.51, −4.97, and −10.22 eV, respectively, which indicates that it is unlikely that the C_7H_7 ligand will exist in a formal 3− valence state. Further, the experimental ionization energies for actinide atoms[70] indicate that the fourth ionization energies of Pa through Am are extremely large, approaching the sum of the first three ionization energies. Thus, although formal An oxidation states of +5 or +6 may be assigned in these systems (*vide infra*), it is apparent that the actual positive charge on the An atom will be considerably less.

We have undertaken Mulliken population analysis[71] of the BP^R charge distributions in the $AnCh_2^q$ complexes; the Mulliken populations are tabulated in the Supporting Information. In nearly all cases, the calculated charge on the An atom is between +2.5 and +3.1 regardless of the overall charge on the complex. For example, the calculated charges on the U atom in UCh_2 and UCh_2^- are +2.54 and +2.53, respectively. As a point of comparison, our calculated charges on U in UF_6 and the UO_2^{2+} ion are +4.77 and +2.44, respectively.[72] Both UF_6 and UO_2^{2+} are considered U(VI) complexes.

We note that the formal charge on U is essentially the same for both UCh_2 and UCh_2^-. This somewhat surprising result implies that the addition or removal of electrons in $AnCh_2$ systems involves primarily the ligand-based electrons. This conclusion is in excellent accord with our earlier analysis of the C−C bond distances, and with the previous conclusions on the nominal Ch charge in transition-metal ChMCp complexes.[12]

Oxidation States in UCh_2 and UCh_2^-. Finally, we will address a more formalistic question, but one that is of great interest to inorganic chemists: What is the best choice of oxidation state for the actinide element in these cycloheptatrienyl sandwich complexes? Because of the intense interest in uranium chemistry, we shall focus on the known UCh_2^- ion and the neutral UCh_2 molecule.

At first glance, UCh_2 might be described as an f^0 U(VI) center interacting with two Hückel aromatic $C_7H_7^{3-}$ rings; like other f^0 complexes, UCh_2 is closed shell and has no electrons residing in U-localized 5f orbitals. By this reasoning, the UCh_2^- would be an f^1 U(V) complex. This is the description that was proposed by Ephritkhine and co-workers in their initial report of the synthesis of UCh_2^-. Although these descriptions are not unreasonable, we think that they are not the best ones for these systems because they neglect the strong U−Ch interactions.

As noted earlier, the $3e_2''$ MO of UCh_2 and UCh_2^- is a nearly equal mixture of the U 5f and Ch π_2 orbitals. In both UCh_2 and UCh_2^-, this MO is filled with four electrons. Because of the nearly equal sharing, it is reasonable for purposes of assigning oxidation states to attribute two of these electrons to the U 5f orbitals and two to the Ch π_2 orbitals. This partitioning scheme would lead to UCh_2 being described as an f^2 U(IV) center interacting with two Ch^{2-} ligands. Likewise, UCh_2^- would be considered an f^3 U(III) complex. It is notable that U(III) and U(IV) are two of the most common oxidation states in organouranium chemistry.

The strong sharing of electrons between the U and Ch orbitals differs somewhat from typical metal−Cp interactions. In most Cp complexes, the M−Cp bonding orbitals are predominantly Cp in character, which leads to the description of the ligand as Cp^-. The situation in UCh_2 is similar to other metal−ring systems, such as $(\eta^4\text{-}C_4H_4)Fe(CO)_3$[73] and $(\eta^8\text{-}C_8H_8)_2Ce$,[8e,h] in which there is nearly equal sharing between the metal and ring orbitals in some of their MOs.

As noted in Figure 8, the An 5f contribution to the $3e_2''$ MO changes substantially as one moves across the actinide elements. The strong An−Ch sharing in this MO is most evident for U, Np, and Pu. Thus, we would assign oxidation states for the Np and Pu complexes in a fashion analogous to that for the U complexes.

Concluding Comments

The successful synthesis and characterization of $[U(\eta^7\text{-}C_7H_7)_2]^-$ opens a new chapter in the organometallic chemistry of the actinide elements. This contribution is intended to chart future directions in this chemistry with the hope that it becomes a more developed area of investigation. Our calculations provide the following guidance: (1) In general, we expect the chemistry of $AnCh_2^q$ complexes to be more successfully developed for the early actinide elements than for the late ones. (2) The fact that the first species in this class is anionic is not surprising. We find that the electron affinities of all the $AnCh_2$ neutrals are positive, indicating that they should be oxidizing species. (3) The An−Ch bonding involves significant interactions between the ring orbitals and both the An 6d and 5f atomic orbitals. (4) Oxidation or reduction of the complexes should involve primarily ligand-based electrons. We hope that spectroscopic studies on these systems, particularly the uranium species, will provide corroboration of this bonding description.

In spite of the efforts put forth here, it is clear that an even more proper description of the ground electronic structures of these molecules and ions will require additional computational effort. In particular, inclusion of spin−orbit coupling will be necessary for the correlation of optical spectra, and the inclusion of non-dynamic electron correlation is indicated because of the presence of near-degenerate configurations in the ground states. Our efforts on these problems are ongoing.

Acknowledgment. We thank Dr. Clinton S. Nash for helpful discussions. We gratefully acknowledge support for this research from the Division of Chemical Sciences, U.S. Department of Energy (Grant DE-FG02-86ER13529), and from the Ohio Supercomputer Center.

Supporting Information Available: Tables of the optimized structures and energies for the ground electron configurations of eclipsed $AnCh_2^q$ (An = Th−Am; q = 2−, 1−, 0, 1+) systems, and of the Mulliken atomic charges, C_7H_7 group charge, and An 5f and 6d total populations for $AnCh_2^q$ systems at the optimized geometries (3 pages). See any current masthead page for ordering and Internet access instructions.

JA971149M

(70) Cotton, S. *Lanthanides and Actinides*; Oxford University Press: New York, 1991.
(71) Mulliken, R. S. *J. Chem. Phys.* **1955**, *23*, 1833; **1962**, *36*, 3428.
(72) Li, J.;. Bursten, B. E Unpublished results.
(73) Bursten, B. E.; Fenske, R. F. *Inorg. Chem.* **1979**, *18*, 1760.